ORIGINAL ARTICLE

Optimization of process parameters for friction stir welding of dissimilar aluminum alloys using different Taguchi arrays

Mohamed Mohamed Abd Elnabi[1] · **Alaa El Mokadem**[1] · **Tarek Osman**[1]

Abstract

A statistical optimization based on experimental work was conducted to consider ultimate tensile strength (UTS) and elongation of dissimilar joints between AA5454 and AA7075 by friction stir weld (FSW). The goal of this work is to develop a comparative study of the optimization of FSW parameters using different orthogonal arrays, i.e., L12 and L16. Four parameters correlated to softening and forging requirements (rotational speed, traverse speed, tilt angle, and plunge depth), one parameter associated with the location of base metal in the dissimilar joint, and two parameters related to an FSW tool (pin profile and $D_{shoulder}/d_{pin}$ ratio) were considered and arranged in the employed arrays. Moreover, the investigation explored the microstructure and fractography of dissimilar joints and base metals by using optical and scanning electron microscopes. The results showed that the L16OA is more accurate than L12OA for the optimization of seven parameters due to the small statistical errors. For UTS, the errors range from 0.78 to 24% for L16OA and from 27.23 to 44.14% for L12OA. For elongation, the errors run from 11 to 12.9% for L16OA and from 33.77 to 49.73% for L12OA. The accuracies of generated models range from 50 to 99.5% for L16OA and range from 30.7 to 94.9% for L12OA. Tightening the levels (narrow domain) is the main reason for switching some optimum levels between both arrays. The highest UTS obtained is 221 MPa based on the optimum levels attained from L16OA, and the highest elongation is 12.83% according to the optimum levels acquired from L12OA. Despite the deficiency of effective intermixing, the study revealed that FSW acceptably could assemble joints between AA5454 and AA7075, presenting the proficiency of FSW with welding dissimilar aluminum alloys.

Keywords Friction stir welding · Optimization · Dissimilar aluminum alloys · Taguchi · L12OA · Response surface methodology · Microstructure · Fractography

1 Introduction

The emergence of joining dissimilar aluminum alloys has a special consideration for numerous emerging applications, including aerospace, power generation, defense, transportation, and shipbuilding [1]. Fabrication of material joints demands a smooth surface finish and reasonable mechanical adequacy [2]. Solid-state processes are particularly attractive for producing joints of dissimilar metals that are difficult to join by traditional fusion techniques. It is required to defeat technological issues induced by significant differences between the metal to be welded in terms of structure,

atomic bonds, and physicochemical properties (e.g., melting points, mechanical properties, coefficients of conductivity, and thermal expansion) [3]. Traditional processes are limited as a film of oxide readily forms on the surface and edges of the aluminum, and this ought to be cleared before joining. Moreover, it is problematic to heat the Al locally due to its high thermal conductivity and expansion, which also drives the joint prone to stresses and deformation. This is why the solid-state welding methods are recommended [4].

Friction stir welding (FSW) is a trendy joining procedure that produces great-characteristic joints by joining materials below their melting temperature. Being such a solid-state process, FSW omits numerous flaws correlated to fusion welding processes like solidification cracking, liquation cracking, distortion, and porosity. A rotating cylindrical tool with a clamped workpiece is a key to implementing the process. The tool consists of a profiled or non-profiled shoulder and a pin. The rotating tool with a thinning contact between

✉ Mohamed Mohamed Abd Elnabi
  mohamed.abd.M@eng-st.cu.edu.eg;
  mohamed.abdelnabi@pg.cu.edu.eg

1 Department of Mechanical Design and Production, Faculty of Engineering, Cairo University, Giza 12613, Egypt

the shoulder and the surface of a material to be welded produces the frictional heat needed. After reaching the plastic deformation mode of materials to be welded, the stirring operation is feasible by the pin. Tool design and machine parameters influence the stirring quality in the weld zone [5]. Recently, FSW has been used to join various metal combinations, e.g., dissimilar aluminum alloys [6, 7], aluminum to brass/copper [8, 9], aluminum to steel [10, 11], aluminum to magnesium [12], and aluminum to titanium [13].

The optimization of process parameters has enhanced the joint quality required. However, inadequate levels of process parameters may induce flaws [14]. Numerous approaches have been utilized for process optimization, e.g., regression analysis, design of experiments (DOE), analysis of variance (ANOVA), response surface methodology (RSM), among others [15]. Lessening the number of trials by DOE techniques minimizes the cost and time required. Taguchi, a most common DOE technique established on orthogonal arrays, has been exceedingly involved as a process optimization mean. Utilizing Taguchi with ANOVA allows estimating the statistical significance of process parameters on responses [14]. RSM is a highly efficient approach for building a mathematical model to predict and represent the relation between parameters and responses [16]. The major weakness of the Taguchi approach is that the influences acquired are only relative and do not exactly demonstrate what parameter holds the highest impact on the response value. It means any change in experimental procedures, parameters, levels, and conditions will change the results and influences. Also, this method should not be utilized when all relationships between all parameters are required due to the array fraction. Another restriction is that the Taguchi is an offline optimization technique and thus unacceptable for a dynamically adjusting operation [17].

Many researchers have performed systematic analyses to optimize process variables on many outputs to estimate welding quality (efficiency), such as strength, hardness, and elongation %. Welding efficiency is estimated by dividing a selected weld property by corresponding base metal property. Each investigation has studied the effect of some parameters and overlooked some (set at fixed values) throughout the optimization process. Anil Kumar et al. [18] examined the impact of rotational speed, traverse speed, and plunge depth of dissimilar AA2024-T351/AA7075-T651 on tensile properties using a bottom-up approach (adjust values of only one parameter and fix the others). The best welding efficiency obtained is 92% of the strength of the softer side. The deficiency of this method outlines in conducting many experiments without realizing which factors are more influential and determining the optimal levels.

Most investigations have been attempted to optimize the key FSW parameters, namely rotational speed, traverse speed, and axial force using different aluminum grades and different arrays on ultimate tensile strength [19–24]. Babu et al. [19] examined similar joints of AA5059 with a thickness of 1 mm using a central composite design of 20 combinations (3 parameters (p):5 levels (L) ($2^3 = 8$)/6 stars/6 centers). The optimal welding efficiency obtained is 76.4% using the levels of 950 rpm, 25 mm/min, and 3.4 KN. Ramaraju et al. [20] examined similar joints for each of AA6061 and AA5083 and dissimilar joints of AA6061/AA5083 with a thickness of 5 mm using Taguchi L8OA (3P:2L ($2^3 = 8$)). The optimal welding efficiencies obtained are 90%, 65%, and 61% for AA6061, AA5083 similar joints (at 1600 rpm, 160 mm/min, and 2.5 KN), and AA6061/AA5083 dissimilar joint (1000 rpm, 40 mm/min, and 3.5 KN), respectively. Murali Krishna et al. [21] examined dissimilar joints of AA6351-T6/AA2024-T6 with a thickness of 5 mm using full factorial design-L27OA (3P:3L ($3^3 = 27$)). The best welding efficiency obtained is 78.8% of the strength of the softer side using the levels of 1200 rpm, 42 mm/min, and 7 KN. Lakshminarayaran and Balasubramanian [22] examined similar joints of AA7039 with a thickness of 6 mm using Taguchi L9OA (3P:3L (1/3 of 3^3)). The optimal welding efficiency obtained is 82.2% using the levels of 1400 rpm, 22 mm/min, and 6 KN. Chanakyan et al. [23] studied AA6082 FSW joints of 6-mm-thick using a face central composite design (CDD) of 20 combinations (3P:3L). The optimal welding efficiency obtained is 71.8% using 1100 rpm, 58 mm/min, and 6 KN. Umanath et al. [24] investigated AA6063 FSW joints of 6-mm-thick using a face CCD of 20 combinations (3 parameters: 5 levels). The results revealed that the contributions of these parameters are very close, about 30.59% RS, 32.4% TS, and 37% AF. The optimal levels are 1000 rpm, 90 mm/min, and 4 KN. These studies reveal that the three parameters are statistically significant in deciding joint strength, except for [20]. They focused on the significance of these parameters under the same levels, same conditions, and the same selected array on different aluminum grades, similar and dissimilar joints. Under these conditions, the results exhibited that the significance of the parameters and the optimal levels may vary. They mentioned that the significant parameters are both speeds for the AA5083 joint, axial force for the AA6061 joint, and traverse speed for dissimilar AA5083/AA6061 joint.

The enlargement of the optimization process has been studied by adding another variable to the key FSW parameters [25, 26]. Palanivel et al. [25] added the pin profile for examination of dissimilar joints of AA6351-T6/AA5083-H111 with a thickness of 6 mm using a CCD of 31 combinations (4P:5L ($2^4 = 16$)/ 8 stars/ 7 centers). The optimal welding efficiency obtained is 85.4% using the levels of 950 rpm, 63 mm/min, 14.7 KN, and a straight square pin profile. Venkateswarlu et al. [26] added shoulder feature for examination of dissimilar joints of AA2219/AA70391 with a thickness of 6 mm using a mixed array (2P:2L and 2P:3L).

The optimal welding efficiency obtained is 80.69% using the levels of 745 rpm, 20 mm/min, 6 KN, and concave shoulder feature. Depending on these studies, the pin profile and shoulder feature are statistically significant besides the three main parameters.

Other optimization studies have substituted the axial force (uncontrollable) by tool plunge depth into the workpiece or keeping it a constant and adding other parameters besides rotational and traverse speeds [27–29]. Jia et al. [27] investigated a similar joint of AA6061-T6 with a thickness of 3 mm using Taguchi L9OA (3P:3L (1/3 of 3^3)). The best welding efficiency obtained is 94% using the levels of 5000 rpm, 3000 mm/min, and 0.25 mm plunge depth. Ahmadnia et al. [28] checked the accuracy of three models for strength, hardness, and elongation on dissimilar joints of AA6061/AA5010 with a thickness of 5 mm using a CCD of 20 combinations (3P:5L ($2^3 = 8$)/6 stars/6 centers). The models are significant for all responses, but all three parameters are statistically insignificant. The results showed that the optimum levels are identical for both hardness and strength (800 rpm, 60 mm/min, and 0.2 mm plunge depth) and vary with elongation (1000 rpm, 40 mm/min, and 0.3 mm). Simoncini et al. [29] obtained a 69.4% of ultimate tensile strength (UTS) on AA6082-T6 (2 mm) using Taguchi L27OA (3P:3L). The plunge depth holds more than 50% of the process contributions.

The optimization of pin profile in addition to rotational and traverse speeds has been also investigated [30–34]. Sefene et al. [30] studied multi-responses of hardness and tensile on AA6061 similar joints with a thickness of 5 mm using gray relation with Taguchi L9OA (3P:3L (1/3 of 3^3)). Sagheer-Abbasi et al. [31] studied the tensile response of AA5052-H32 similar joints with a thickness of 1 mm using Taguchi L9OA (3P:3L (1/3 of 3^3)). Meengam and Sillapasa [32] used a full factorial design of L64OA (3P:4L) for the optimization of AA6063 (6 mm) FSW joints. Balamurugan et al. [33] studied the tensile response of dissimilar joints of AA5052-H32/AA6061-T6 with a thickness of 5 mm using Taguchi L27OA (3P:3L). Raj et al. [34] used L9OA to optimize the parameters of AA3013/AA7075 dissimilar joints. The significance of the speeds dominates in deciding the joint strength with a contribution percentage of 91% [30] and 85% [34] compared to the pin profile, but the pin profile monopolizes the output contribution by 51% [31] and 82.17% [33].

In addition to rotational speed, traverse speed, and pin profile, Hasan et al. [35] added tilt angle, and Koilraj et al. [1] added $D_{shoulder}/d_{pin}$ ratio during the optimization process. Hasan et al. [35] constructed a second-order polynomial model with 10% error for tensile strength of dissimilar joints of AA6061/AA7075 with a thickness of 3 mm using a CCD of 31 combinations (4P:5L ($2^4 = 16$)/ 8 stars/ 7 centers). All the selected parameters are statistically significant in tensile

strength. The optimal welding efficiency obtained is 82% using the levels of 1100 rpm, 300 mm/min, 3° tilt angle, and a tapered pin. Koilraj et al. [1] analyzed the tensile strength of dissimilar joints of AA2219-T87/AA5083-H321 with a thickness of 6 mm by Taguchi L16OA (4P: 4L (1/16 of 4^4)). The highest efficiency obtained is 90% using the levels of 700 rpm, 15 mm/min, 3 D/d, and a cylindrical threaded pin. The investigation revealed that only the D/d ratio is the most contributing parameter on the output by 60%.

Furthermore, different combinations of FSW parameters or considering more than four parameters have feasible for optimization. Kumar and Kumar [2] used gray relation with Taguchi L9OA to optimize multi-responses of strength and elongation on dissimilar joints of AA6061/AA6082 with a thickness of 7.5 mm. The parameters picked are pin profile, tilt angle, and rotational speed. At 1550 rpm, 4° tilt angle, and an octagonal pin, the highest efficiencies obtained for tensile strength and elongation are 93% and 79.3%, respectively. The analysis indicated that the rotational speed holds the most contribution to multi responses by 92.24%. Vidal and Infante [36] optimized pin length, traverse speed, and axial force on multi responses of tensile strength, bending strength, and hardness of AA2024-T351 similar joint with a thickness of 4 mm using Taguchi L9OA (3P:3L (1/3 of 3^3)). Pin length is statistically significant for tensile strength by 42.68%, while the traverse speed is for bending and hardness by 45% and 53%, respectively. At different levels, the highest efficiencies obtained for tensile strength, bending strength, and hardness are 66.45%, 68.40%, and 85.41%, respectively. Haribalaji et al. [37] optimized pin profile, traverse speed, rotational speed, tilt angle, and axial force on a single response of tensile strength of AA2024/AA7075 dissimilar joint with a thickness of 4 mm using Taguchi L27OA (5P:3L (1/9 of 3^5)). Pin profile and tilt angle are statistically significant for tensile strength by 37.9% and 31.14%, respectively. Silva et al. [14] explored the effect of rotational speed, traverse speed, tilt angle, plunge depth, D/d ratio, and weld run distance on tensile strength of AA6082-T6 similar joints with different joint configurations. They used Taguchi L27OA for 3-mm butt and T-joints and Taguchi L8OA for 2-mm lap joints. They stated that each joint configuration has distinct parameter levels due to different requirements of heating and flux in the weld zone. Both speeds are statistically significant for the lap joint, but only rotational speed is for the T joint. For the butt joint, the most contributing parameters to the tensile strength are plunge depth and the D/d ratio. Abd Elnabi et al. [38] optimized the most considerable number of FSW parameters on tensile strength and elongation of a dissimilar joint of AA7075/AA5454 with a thickness of 3.5 mm using Taguchi L16OA (7P:2L (1/8 of 2^7)). They investigated rotational speed, traverse speed, tilt angle, location of base metal, D/d ratio, pin profile, and plunge depth. Excluding rotational speed, which only significantly

influences tensile strength, only three parameters are statistically significant to all outputs; speed traverse speed, plunge depth, and D/d ratio. The most contributing parameters to tensile strength and elongation are traverse speed and D/d ratio by 16.9% and 21.4%, respectively. The optimum levels are identical for both responses except for tilt angle and pin profile.

As mentioned earlier, the literature has focused on studying the optimization of FSW parameters by various aspects such as aluminum grades, metal thickness, similar or dissimilar joints, optimization approach, orthogonal array, joint configurations, number of parameters, and parameter combinations. The essence of parameters may differ based on these items. The literature lacks to explore the extent of the consequences of array assignment on the output findings under the same conditions. The novelty of this work is to develop a comparative study of the optimization of FSW parameters using different orthogonal arrays under the same conditions. The purpose is to discover how the selected arrays affect the contribution of parameters to the process, the accuracy of models, obtaining the optimum levels, and the deviations between the predicted and experimental results based on the level of the fraction selected. The comparisons are between the results of this research using Taguchi L12OA and the results of the Abd Elnabi et al. [38] using Taguchi L16OA. Moreover, the investigation explored the microstructure and fractography of dissimilar joints and base metals.

2 Materials and methods

A heat treatable aluminum alloy of 7075 and a strain hardening aluminum alloy of 5454 were base metals used in this work. X-ray fluorescence spectrometer (XRF) was used to examine the chemical compositions of the metals used. Table 1 clarifies the chemical compositions and mechanical properties of both alloys. For standardization, the base metals were machined to $138 \times 81 \times 3.5$ mm by a vertical milling machine. AA7075 has numerous applications in the aerospace, defense, marine, and automobile due to the high S/W ratio and acceptable corrosion resistance, with apprehension related to reliability and lifetime when positioned in variable marine environments. Joining this alloy with another that retains excellent corrosion resistance in marine atmospheres will be valuable in such cases. AA5454 is one of these alloys. The uses of AA5454 are in all sorts

of welded assemblies, tanks, pressure vessels, trucking, and dump bodies [39, 40].

The study relied on the same parameters and levels as the Abd Elnabi et al. [38]. Four parameters correlated to softening and forging requirements (rotational speed, traverse speed, tilt angle, and plunge depth), two parameters related to an FSW tool (pin profile and $D_{shoulder}/d_{pin}$ ratio), and one parameter associated with the location of base metal in a dissimilar joint were used and arranged in the employed array-Taguchi L12 orthogonal array. Table 2 illustrates the arrangement of the parameters and their levels in Taguchi L12OA.

Four different shapes represented the tool parameters in L12OA used. Figure 1 shows a simple drawing of the four tools used in this study. The tools consisted of a tapered pin profile were combined with a concave surface shoulder. Up to 1 mm from the tool circumference, the surface was flat, and then an internal concave of 10° was machined to the center. The tools consisted of a cylindrical pin profile were combined with a flat surface shoulder. The length of all pins was 3.2 mm. The material used to fabricate the four tools was hot-worked tool steel of H13. Then, the tools hardened by heat treatment according to the BÖHLER standard [11]. The hardness gained after heat treatment was 50–53 HRC.

Figure 2 shows machine used (a), sheet dimensions with clamp positions (b), welded joints after machining of test specimens (c), and test specimens (d). The joints were carried out by a classic WMW ECKERT vertical milling machine (Fig. 2a). The sheets were fixed above a steel backing plate using two clamps, as shown in Fig. 2b. The process required four tool actions to complete, namely rotation, penetration and plunging, translation, and retraction. A tachometer was utilized to calibrate the speeds.

Ultimate tensile strength (MPa) and elongation % were the outputs utilized to assess the process. Transverse tensile specimens were taken according to ASTM B557-Sub size to assess the strength of joints [41]. A computerized universal testing machine was employed to accomplish the tensile test. All specimens were machined using a wire cut machine. Two microscopes were used to examine microstructure and fractography, namely an Olympus optical microscope (OM) and a Quanta 250 FEG scanning electron microscope (SEM). The specimens were prepared according to metallography standard ASM-9 [42]. Silicon carbide abrasive papers beginning at 180 grit and progressing through 240, 320, 400, 600, 800, 100, 120, and 1500 were used for grinding. Then, the specimens were polished using 1 μm diamond

Table 1 The chemical compositions of base aluminum alloys used and mechanical properties

| Alloy | Element (wt. %) | | | | | | | | | Properties | | |
	Cr	Cu	Fe	Mg	Mn	Si	Ti	Zn	Al	UTS (MPa)	YS (MPa)	Elongation %
AA7075	0.28	1.59	0.16	1.61	0.05	0.27	0.09	5.18	90.65	402	358	10
AA5454	0.20	0.04	0.21	2.50	0.96	0.25	-	0.12	95.22	260	180	4

Table 2 Experimental plan according to Taguchi L12OA

Control variables (L12OA) ** Column number in L12OA

No	Rotational speed (rpm) X1		Traverse speed (mm/min) X2		Pin profile based on taper angle (°) X3			D/d ratio X4		Tool tilt angle (°) X5		Location of base metal (Softer) based on tool rotation direction (°) X6			Plunge depth (mm) X7	
**	1		2		3			4		5		6			9	
1	1	1000	1	17	1	Cylindrical	0	1	3	1	1.5	1	Retreating	CCW -360	1	0.1
2	1	1000	1	17	1	Cylindrical	0	1	3	1	1.5	2	Advancing	CW +360	2	0.25
3	1	1000	1	17	2	Tapered	17	2	4	2	2	1	Retreating	CCW -360	2	0.25
4	1	1000	2	21	1	Cylindrical	0	2	4	2	2	1	Retreating	CCW -360	1	0.1
5	1	1000	2	21	2	Tapered	17	1	3	2	2	2	Advancing	CW +360	1	0.1
6	1	1000	2	21	2	Tapered	17	2	4	1	1.5	2	Advancing	CW +360	2	0.25
7	2	1225	1	17	2	Tapered	17	2	4	1	1.5	1	Retreating	CCW -360	1	0.1
8	2	1225	1	17	2	Tapered	17	1	3	2	2	2	Advancing	CW +360	1	0.1
9	2	1225	1	17	1	Cylindrical	0	2	4	2	2	2	Advancing	CW +360	2	0.25
10	2	1225	2	21	2	Tapered	17	1	3	1	1.5	1	Retreating	CCW -360	2	0.25
11	2	1225	2	21	1	Cylindrical	0	2	4	1	1.5	2	Advancing	CW +360	1	0.1
12	2	1225	2	21	1	Cylindrical	0	1	3	2	2	1	Retreating	CCW -360	2	0.25

Fig. 1 The FSW tools used in this study
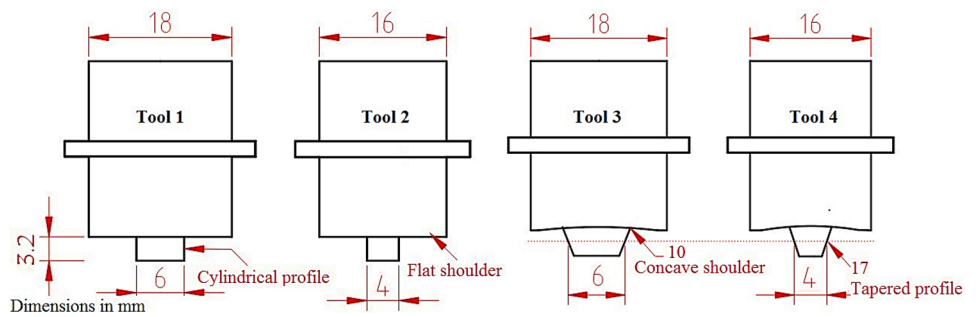
Fig. 2 WMW ECKERT machine used (**a**), clamping system (**b**), welded joints after machining of test specimens (**c**), and test specimens (**d**)
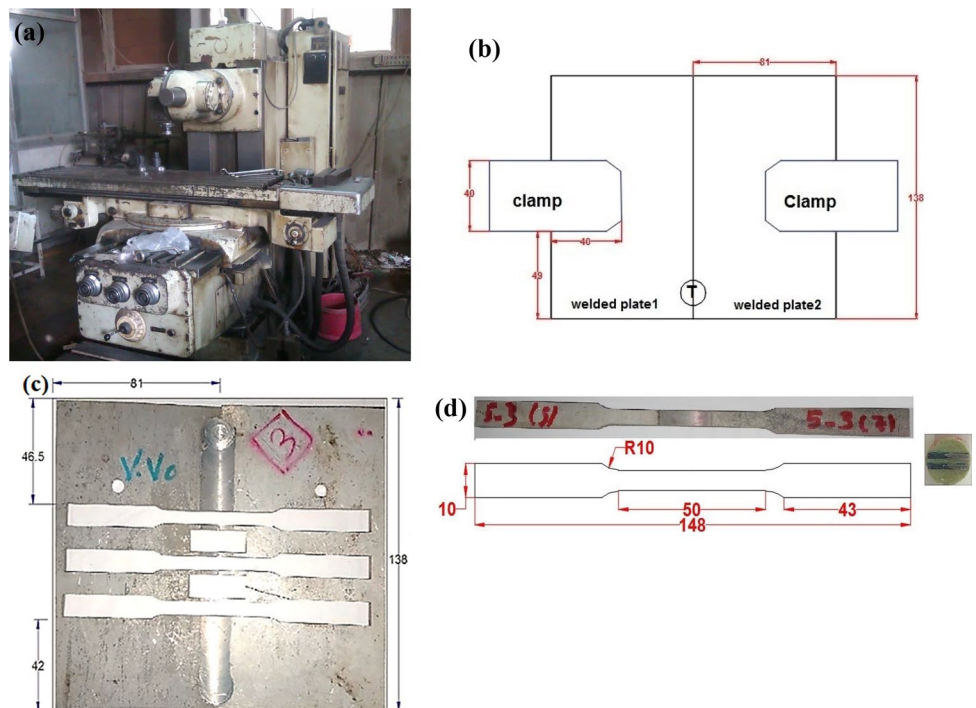
paste and 0.3 μm Al_2O_3. The etchants used are 4 M Keller for macrostructure (20 ml distilled water, 20 ml HCL, 20 ml HNO_3, and 5 ml HF) for 5–10 s and Keller for microstructure (190 ml distilled water, 3 ml HCL, 5 ml HNO_3, and 2 ml HF) for 30 s.

3 Results and discussions

3.1 Optimization of experimental results based on Taguchi L12OA

The main objective of the Taguchi method is to design a robust system that is reliable under noise parameters. This method adjusts design parameters to their optimal levels that making the process to be insensitive to the noises. The noise parameters are either not controllable or too hard (expensive) to control [43]. The motivation of using the signal to noise (S/N) ratio is to realize a state under which the influences of controllable parameters can eliminate or weaken the noises' effect (uncontrollable). The S/N criterion, higher is better, is employed to maximize the outputs (strength and elongation) to uncontrollable noises. Based on this criterion, the levels which produce the highest ratio are optimum. It can be obtained as follows [44]:

$$\frac{S}{N} ratio = -10 \log_{10} \left(\frac{1}{n} \sum_{i=1}^{n} \frac{1}{y_i^2} \right) \quad (1)$$

where y_i is the ith observation of a treatment combination and n is the number of replications.

The results of UTS and elongation achieved based on the array arrangements are given in Table 8 (Appendix). Figure 3 gives the mean, standard deviation (SD), and S/N ratio of UTS (MPa) and elongation %. The domain of UTS results runs from 165.003 MPa at trial No. 11 (T11) to 212.193 MPa at T2. The joint efficiency ranges from 63.5 to 81.6%,

compared to the strength of the softer side (AA5454). The elongation ranges from 4.266 (T11) to 11.7333% (T8). By comparison with AA5454 side, the elongations are between 106.65 and 293.33%. The domain of the S/N ratio based on UTS results is from 44.20 at T11 to 46.53 at T2. Also, for elongation, it varies from 12.5077 at T11 to 21.3256 at T2. Hence, the extent of variation is very small by 2.33 in the UTS, but it is relatively large by 8.81 in the elongation. The significant difference in S/N ratios means that the noises may affect the process, but this method allows the process to be insensitive to noises if controlling the optimum levels or/and significant parameters. Based on the results of UTS, the SD varies from 30.5917 at T9 to 1.8113 at T6. Based on the elongation results, the SD varies from 5.6083 at T9 to 0.4618 at T11. Hence, the variation is very high. The trials showing a small SD indicate that the data sets cluster near the mean of UTS/elongation. Also, the trials displaying a large SD reveal that the data sets spread far from the mean resulting in low precision. For example, each of the two UTS sets {T2: 206,207.04,223.54}, {T6: 210.50, 214.03, 211.56} has a mean of ~212 MPa. Their SDs are 9.8403 and 1.8113, respectively. The second set has a much smaller SD than the first set because its values are close to the mean of 212 MPa.

The most probable noise in FSW is an uncontrollable axial force that appears if using a traditional milling machine. The use of the plunge depth without force controller may result in forming some defects or producing different weld qualities in the same operation depending on surface conditions of a workpiece and machine linkages deflect under loading conditions. Thus, the tool cannot adjust its position during the process with more digging into the workpiece, causing a significant amount of weld flash. In contrast, the force controller can revise the position of the tool by keeping it at a constant contact force and preventing the flash problem. Also, it explains why the results may relatively varies at the same trial [45].
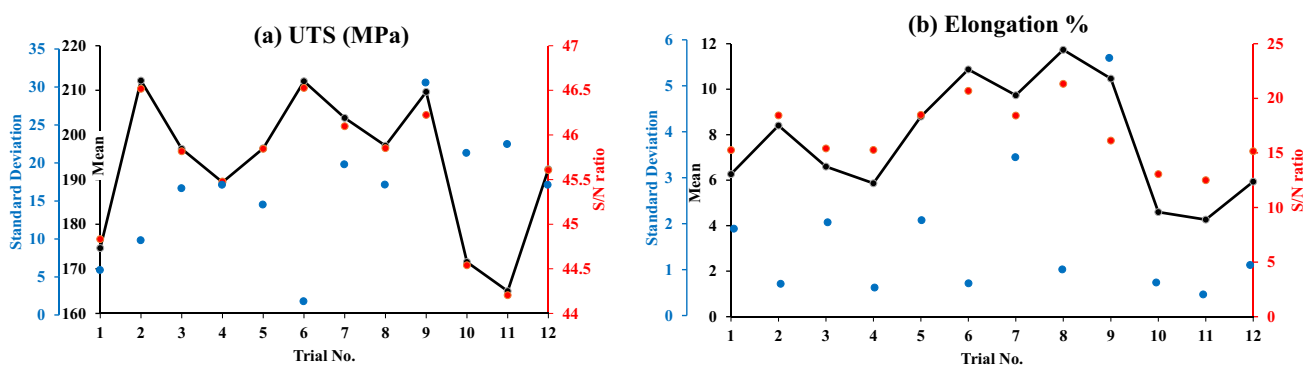

Fig. 3 The mean, S/N ratio, and standard deviation of experimental UTS (**a**) and elongation (**b**)

3.1.1 Main effects of process parameters on UTS and elongation

Figures 4 and 5 represent the main effects of each parameter (and each level) on the tensile strength and elongation, respectively. These plots describe the mean, S/N ratio, and standard deviation of the responses versus factor level. The study of linear effects is only permitted based on the L12OA, which depends on a two-level parameter. Graphically, each bar depicts the extent of the differences in the output results at each level. The lengthy the bar, the higher effect of the parameter. The UTS and elongation of the joints increase with increasing the levels of all selected parameters, excluding both speeds. The changes in tensile results between the two levels of each parameter, between 6 and 11.3 MPa, are relatively less sensitive due to tightening the levels of the parameters. It is approximately 4% of the strength of the AA5454. Also, the differences in S/N ratio-UTS are very small with a variation between 0.2 and 0.52,

with changing of all parameters. Furthermore, Fig. 4 indicates that three parameters are the most significant on the UTS (mean/S/N ratio), namely, traverse speed, base metal location, and plunge depth. For SD-UTS, only rotational speed, tilt angle, and D/d ratio show the most influences. The changes in elongation results, between 0.01% and 2.59%, are more sensitive to the influences of some parameters. It is approximately 64.75% of the elongation of the AA5454. Figure 5 reveals that the traverse speed, location of base metal, and pin profile are the most significant parameters on (S/N ratio and mean) elongation. Also, the differences in S/N ratio-elongation are more observed than that of UTS, with a variation between 0.399 and 2.49. For SD-elongation, traverse speed is still the most significant parameter with the highest variation on output by SD of 1.5. Also, the D/d ratio is contributed to SD with 1.13.

The tensile properties increase with decreasing the rotational and traverse speeds. Discussing the improvement of tensile strength based on the amount of heat input produced
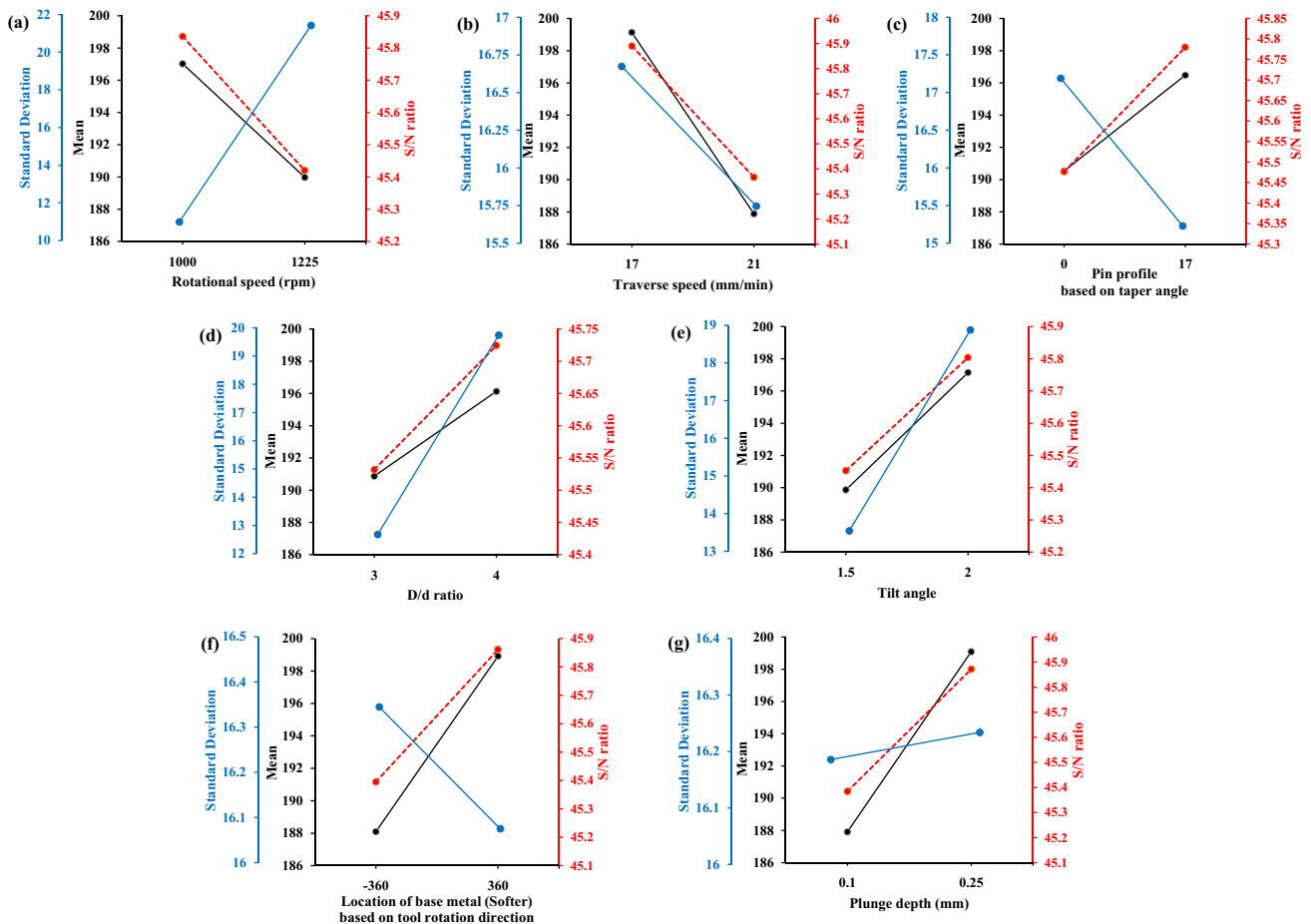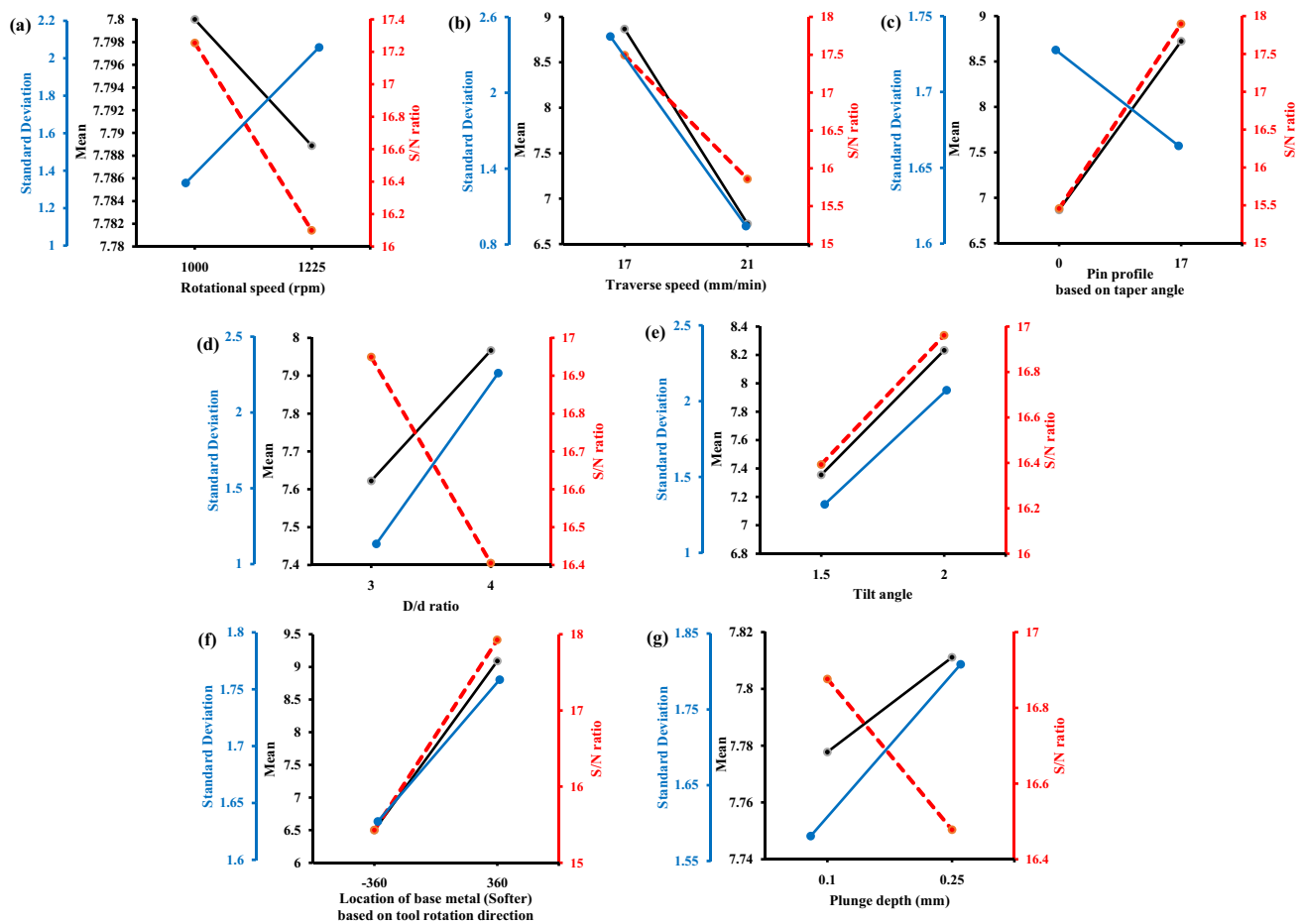

Fig. 4 The influences of seven FSW parameters optimized on UTS based on L12OA

Fig. 5 The influences of seven FSW parameters optimized on elongation % based on L12OA

by both speeds may be feasible [46]. Both conditions of rotational speed (i.e., high, or low) may negatively contribute to the joint strength. It should be optimized with other parameters, specifically with the traverse speed [14]. During FSW, it is not preferred to use undesirable low or high heat input. If the high heat input exceeds the normal limit, the joint strength decreases due to the turbulence in metal flow (destroys the regular flow) and the grain coarsening. The high heat input with a proper value of the speeds' combinations results in adequate stirring since the alloys became more plasticized (softer) [19, 46]. In contrast, using low heat input reduces the consolidation of transferred materials [19]. A low tool feed may expand frictional heat and diminish the cooling rate, resulting in a drop in tensile strength. This effect is observed when combined with high rotational speed. Also, this directs to grain growth [18]. A high tool feed may result in low frictional heat, resulting in a deficiency of metallurgical bonding between both alloys and building a sharp boundary between different weld zones. This leads to a decrease in joint strength [47]. The optimum traverse speed contributes to a rapid cooling rate that

lessens the metallurgical changes through the process, such as re-precipitation, solubilization, and grain coarsening [48]. It should control the heat input by keeping it at the optimum limit which is not remarkably at a low or high heat input [46]. It is not convenient to ignore the influence of the D/d ratio here in generating frictional heat and relying only on the speeds. The UTS increases with the increase of the D/d ratio. The first ratio of 3 produces more heat than the second ratio of 4. This is due to a higher shoulder diameter (18 to 16 mm) and a smaller pin diameter (6 to 4 mm). The optimum condition obtained is at low levels of both speeds with the D/d ratio of 4. This condition represents the proper heat by a combination of high heat by low traverse speed and low heat by the low rotational speed with the small shoulder diameter.

Low plunge depth creates inadequate forging and frictional heat resulting in defects [28]. A good contact by the proper plunge depth provides the amount of frictional heat needed to sustain the metal flow. Hence, the tensile properties of joints increased at 0.25 mm [49]. Also, when plunging goes beyond the required depth, the thinning in

the weld zone becomes higher. The reduction in weld thickness reduces the joint strength [28]. Normally, more heat input generated using high speeds ratio with a high plunge depth results in the coarsening of the grains in the weld zone. Proper shoulder thinning is critical to the tensile properties [27].

The objective of a pin is to stir materials from side to side, to make the intermixing between both materials at the contact line, and to increase the heat in the bottom region of the weld [50]. In this study, one of the lowest contributing parameters on tensile strength is the pin profile. It may be due to the insufficient stirring produced by both pins. Using the cylindrical and tapered pins without thread gives a minimum metal flow in the vertical direction, but the thread exhibits a big welding problem (oxide layer inclusion) [50]. The threaded tapered pin gives more velocity for stirring in the vertical direction [5]. The objective of the concave on the shoulder surface is to maintain the deformed material in the weld zone by preserving the deformed material in the concave region and feeding them again by the tool action. The flat and the convex shoulders stir fewer deformed materials than the concave shoulder under the shoulder region [50]. The proper concave angles have been operated between 6° and 10°. The proper operation of this shoulder design requires tilting the tool 2 to 4° from the normal direction of the workpiece to the feed direction [5, 50]. The results reveal that the tool which possesses the shoulder concavity of 10° with tilting by the angle of 2° gives the most impact on the tensile properties. The tool was tilted to increase the pressure on the trailing edge of the tool (the side of the weld). This pressure helps to forge the deformed metals correctly.

The location of each base metal on dissimilar joints influences the intermixing of both alloys in the nugget. The advancing side (AS) is a side where the speeds are in the same direction, and the opposite side is the retreating side (RS). If using two metals with an enormous difference in properties, particularly plasticized temperature, normally the hard metal is located on the AS due to the ease of flowing it into the soft metal at the inactive area (at the front of the tool) [10, 11]. Different results have been observed when joining metals with close properties as dissimilar aluminum alloys. The effects reveal that when AA5454 (softer) was put on the AS, the intermixing is relatively more effective with reflecting on high tensile strength. The strength of the joint increased by 10.8 MPa (4% of the strength of AA5454). The same results were observed when positioning the low strength on the AS; AA6061 of dissimilar AA6061/AA7075 [52] and AA5052-H32 of dissimilar AA6061/AA5052 [53]. Msomi and Mabuwa [51] reported that the tensile properties of dissimilar AA1050/AA6082 welds were not influenced by the material positioning. The differences in strength and elongation were < 2 MPa and 0.4%, respectively. It may be due to the inaccurate levels, as the efficiency was less than 50%. There is a significant concern of rotational speed on metal flow which affects the intermixing. Rodriguez et al. [54] observed insufficient intermixing at low rotational speeds. Dinaharan et al. [55] and Priya et al. [56] indicated that the metal occupation on the weld zone depended on the metal location. The alloy placed on the RS occupied the nugget at low rotational speeds with improper stirring. On the opposite, increasing the speed at specified values reversed the metal occupation to the AS with proper stirring. Also, at the maximum rotational speed, the strength was unaffected by the metal location. Kalemba-Rec et al. [57] reported that it could obtain a proper stirring when placing the harder aluminum on the AS but at a maximum heat input. Since the frictional heat generated on the AS is hotter than that on the RS, the presence of various defects is more attainable due to abnormal material stirring. However, the effect of material location on tensile strength was negligible, about 2% [57].

As shown in Figs. 4 and 5, the optimal levels obtained to maximize the outputs (i.e., UTS and elongation) are similar for mean and S/N ratio except for two levels in the S/N ratio of elongation. The optimum joint should be produced using the speeds' combination of 1000 rpm and 17 mm/min, with tilting and plunging the tool by the angle of 2° and the depth of 0.25 mm, respectively. Also, the tool should have a 16 mm shoulder diameter and 4 mm pin diameter with the tapered profile machined at an angle of 17°. The location of AA5454 base metal is on the advancing side. The confirmation experiments were carried out using the optimum levels. The average values of the UTS and elongation of AA5454/AA7075 joint were 220.006 MPa (S/N ratio of 46.8303) and 12.3% (S/N ratio of 21.7931), respectively.

3.1.2 ANOVA for Taguchi L12-OA

Analysis of variance (ANOVA) is a statistical procedure managed to recognize significant parameters by interpreting the output relative to the statistical deviation. The mathematical calculations according to ANOVA procedures for the parameters' effects on UTS and elongation are given in the Appendix. Tables 9, 10, 11, 12, 13, 14 illustrate the ANOVA tables for mean, S/N ratio, and standard deviation for UTS and elongation. Table 15 indicates the degree of freedom of parameters/errors and the significance degree based on F values at different confidence levels (C.Ls.).

The outcomes of ANOVA are illustrated as follows:

- All the tested parameters are insignificant at any of 90%, 95%, or 99% C.Ls. on elongation for S/N ratio, standard deviation, and the mean.
- Also, All the parameters are insignificant at any of 95% or 99% C.Ls. on UTS for all. At only 90% C.L., the rotational speed is the significant parameter in affecting the standard deviation of UTS.

- Figure 6 reveals the contribution percentage % of the parameters on UTS and elongation for all statistical analyses. Traverse speed, plunge depth, and location of base metal are the most contributing parameters on UTS for both mean and S/N ratio. Traverse speed holds the contributions of 13.66% and 13.26%, plunge depth holds the contributions of 13.47% and 11.48%, and the location of base metal holds the contributions of 12.57% and 10.6% for mean and S/N ratio, respectively. However, the most contributing parameters on SD-UTS are rotational speed, D/d ratio, and tool tilt angle with the percentages of 50.83%, 6.56%, and 4.96%, respectively. The location of base metal, traverse speed, and pin profile are the most contributing parameters on elongation for both mean and S/N ratio. Traverse speed has contributions of 19.48% and 9.39%, pin profile has contributions of 14.58% and 20.83%, and the location of base metal has contributions of 28.39% and 21.82% for mean and S/N ratio, respectively. However, the most contributing parameters on SD-elongation are traverse speed, D/d ratio, tilt angle, and rotational speed with the percentages of 26.84%, 9.56%, 6.77%, and 6.25%, respectively.
- With these results about the significance of the parameters, the insignificant parameters or the lowest contributing parameters should be pooled. Eliminating the effect of these parameters may clarify the proper degree of significance or may shift the insignificant to significant parameters. The pooling procedures are being integrated into each ANOVA table in the Appendix. The theory begins with eliminating the lowest influential parameter, then adding one element after another, and ends when all factors are being eliminated or other results are explored. After pooling, the results did not give many transformations except for three shifts. First, the significance of the rotational speed on SD-UTS turns from C.L. 90 to 99%. Second, the location of base metal becomes significant on elongation at 90 and 95% C.Ls. for S/N ratio and mean, respectively. Third, traverse speed becomes significant on elongation at 90% C.Ls. for standard deviation and mean.

- Statistical errors obtained for S/N ratio, mean, and SD are very high about 44.14% (with pooling 86.74%), 42.33% (with pooling 57.48%), and 35.38% (with pooling 49.15%) for UTS and 40.56% (with pooling 57.35%), 33.77% (with pooling 37.55%), and 49.73% (with pooling 60.72%) for elongation, respectively.

3.1.3 Response Surface Methodology (RSM)

The mathematical model generally used for the process responses is represented as:

$$Y = F\ (X1, X2,\ \dots Xn) + £ \tag{2}$$

where Y, response (output); X, process variable; £, noise or error value.

The coefficient of process parameters using RSM is represented as:

$$[B]\ =\ \text{Inverse}\ ([Z]T * [Z]) * [Z]\text{T} * [F] \tag{3}$$

where $[B]$, array of coefficients of process parameters; $[Z]$, orthogonal array with values of selected process parameters; $[F]$, array with values of measured response; and $[Z]^{T}$, transpose array of $[Z]$.

The deviation between experimental and predicted results can be estimated as Eq. 4.

$$\text{Deviation}\ =\ [(\text{Absolute}\ [R_{\text{measured}} - R_{\text{predicted}}])/(R_{\text{measured}})] \times 100 \tag{4}$$

where R, response

All the mathematical models and 3D surface plots were created by using the MATLAB application. Three mathematical models were built for each response (UTS and elongation). The models were developed based on the results of mean, standard deviation, and S/N ratio. Normally, the models have been generated by inserting only the influential parameters, but the results obtained from the ANOVA tables gave no or at most one significant parameter. According to these results, the models were built with the parameters having the most contributions. For comparison, the full models,
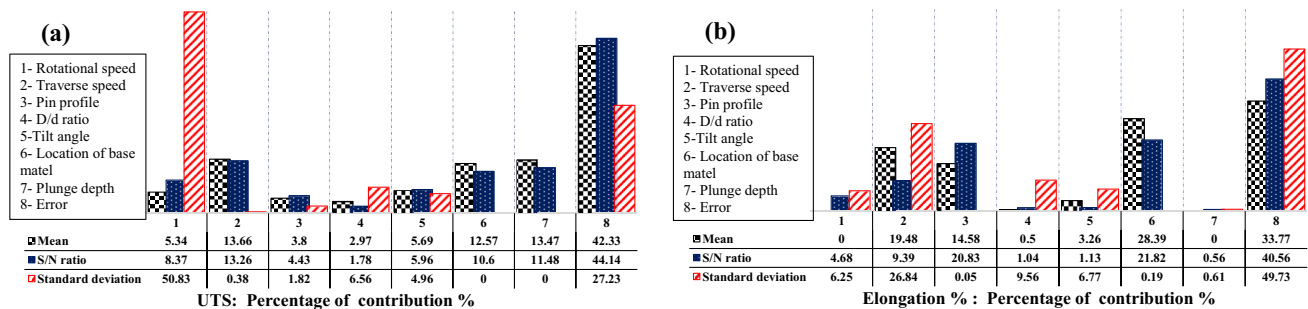

(a)	1	2	3	4	5	6	7	8
Mean	5.34	13.66	3.8	2.97	5.69	12.57	13.47	42.33
S/N ratio	8.37	13.26	4.43	1.78	5.96	10.6	11.48	44.14
Standard deviation	50.83	0.38	1.82	6.56	4.96	0	0	27.23

1- Rotational speed
2- Traverse speed
3- Pin profile
4- D/d ratio
5- Tilt angle
6- Location of base matel
7- Plunge depth
8- Error

UTS: Percentage of contribution %

(b)	1	2	3	4	5	6	7	8
Mean	0	19.48	14.58	0.5	3.26	28.39	0	33.77
S/N ratio	4.68	9.39	20.83	1.04	1.13	21.82	0.56	40.56
Standard deviation	6.25	26.84	0.05	9.56	6.77	0.19	0.61	49.73

1- Rotational speed
2- Traverse speed
3- Pin profile
4- D/d ratio
5- Tilt angle
6- Location of base matel
7- Plunge depth
8- Error

Elongation % : Percentage of contribution %

Fig. 6 Distributions of the contribution percentages % of the process parameters on **a** UTS and **b** elongation

including all selected parameters, were developed for each one. The mathematical representatives (models) of the tensile strength (i.e., Eqs. 5–7 for full models and Eqs. 8–10 for significant models) and elongation (i.e., Eqs. 11–13 for full models and Eqs. 14–16 for significant models) were employed to plot the surface response. These equations represent three analysis aspects (i.e., mean, SD, and S/N ratio) of both responses.

$$UTS_{Mean} = 221.92 - 0.031 * (X1) - 2.81 * (X2) \\ + 0.35 * (X3) + 5.26 * (X4) + 14.55 * (X5) \\ + 0.015 * (X6) + 74.52 * (X7)$$
(5)

$$UTS_{S/N\ ratio} = 47.55 - 0.002 * (X1) - 0.013 * (X2) \\ + 0.018 * (X3) + 0.19 * (X4) + 0.70 \\ * (X5) + 0.001 * (X6) + 3.25 * (X7)$$
(6)

$$UTS_{SD} = -61.96 + 0.05 * (X1) - 0.23 * (X2) \\ - 0.12 * (X3) + 3.78 * (X4) + 10.66 * (X5) \\ - 0.001 * (X6) + 0.32 * (X7)$$
(7)

$$UTS_{Mean} = 233.93 - 2.81 * (X2) + 14.55(X5) \\ + 0.015(X6) + 74.52(X7)$$
(8)

$$UTS_{S/N\ ratio} = 49.6029 - 0.002 * (X1) - 0.013 * (X2) \\ + 0.001 * (X6) + 3.25 * (X7)$$
(9)

$$UTS_{SD} = -67.289 + 0.05 * (X1) + 3.78 * (X4) + 10.66 * (X5)$$
(10)

$$Elongation_{Mean} = 12.79 - 0.0 * (X1) - 0.54 * (X2) \\ + 0.11 * (X3) + 0.34 * (X4) + 1.76 * (X5) \\ + 0.004 * (X6) + 0.22 * (X7)$$
(11)

$$Elongation_{S/N\ ratio} = 29.34 - 0.01 * (X1) - 0.41 * (X2) \\ + 0.14 * (X3) - 0.54 * (X4) + 1.14 \\ * (X5) + 0.004 * (X6) - 2.66 * (X7)$$
(12)

$$Elongation_{SD} = -0.76 + 0.003 * (X1) - 0.38 * (X2) \\ - 0.004 * (X3) + 0.89 * (X4) + 1.51 \\ * (X5) + 0.0002 * (X6) + 1.51 * (X7)$$
(13)

$$Elongation_{Mean} = 17.0528 - 0.54 * (X2) + 0.11 * (X3) \\ + 0.004 * (X6)$$
(14)

$$Elongation_{S/N\ ratio} = 15.4570 + 0.14 * (X3) + 0.004 * (X6)$$
(15)

$$Elongation_{SD} = -0.5270 + 0.003 * (X1) - 0.38 * (X2) \\ + 0.89 * (X4) + 1.51 * (X5)$$
(16)

The distributions of the deviation between predicted results generated from the mathematical equations and the actual results are given in Fig. 7a–f. Each model varies within two percentages, namely, percentage of lowest deviation (LDP) and percentage of highest deviation (HDP). The gap between them constitutes the model accuracy. The lower the gap, the higher the accuracy. For mean-UTS, by the full model, the HDP and LDP are 9.210% (trial (T) 11) and 0.126% (T9), respectively. By the significant model, they are 13.75% and 0.225%. For S/N ratio-UTS, by the full model, the HDP and LDP are 7.30% (T11) and 2.70% (T7), respectively. By the significant model, they are 7.82% and 2.57%. For SD-UTS, by the full model, the HDP and LDP are 377.07% (T6) and 2.03% (T7), respectively. By the significant model, they are 463.39% and 4.025%. For mean-elongation, by the full model, the HDP and LDP are 60.84% (T11) and 2.868% (T8), respectively. By the significant model, they are 66.188% (T11) and 0.225% (T5). For S/N ratio-elongation, by the full model, the HDP and LDP are 20.015% (T11) and 2.64% (T2), respectively. By the significant model, they are 33.65% (T11) and 3.67% (T5). For SD-elongation, by the full model, the HDP and LDP are 191.75% (T11) and 12.62% (T6), respectively. By the significant model, they are 193.86% and 9.26%.

The expected responses have good and relatively high agreements compared with the experimental results. These patterns constitute the model's accuracy. Table 3 gives the accuracies of all models developed. The accuracies of models of both UTS and elongation based on the mean and S/N ratio are relatively high. The accuracies of models are between ~80 and ~96%. The accuracies of full and significant models are very close which allows controlling only the most contributing parameters. These models may give valuable predictions. However, for the standard deviation of both responses, the models are inaccurate due to high deviations. Their accuracies are between ~29 and ~51%. These models may give a highly deviated prediction from the true yield.

Surface response graphically may be drawn in the 3D structure to increase the ability to understand the surface modeling by a clear graphic vision. All the following 3D surface plots were created from the mathematical equations of the UTS and elongation results (S/N ratio and mean). From any plot, it can observe the relation between any two effects on one response. Also, it can predict the output under a condition within the selected domain. The surface plots include two varying parameters with keeping the others at optimum levels. Figures 8, 9, and 10 depict 3D surface plots describing the effect of the significant parameters on tensile strength
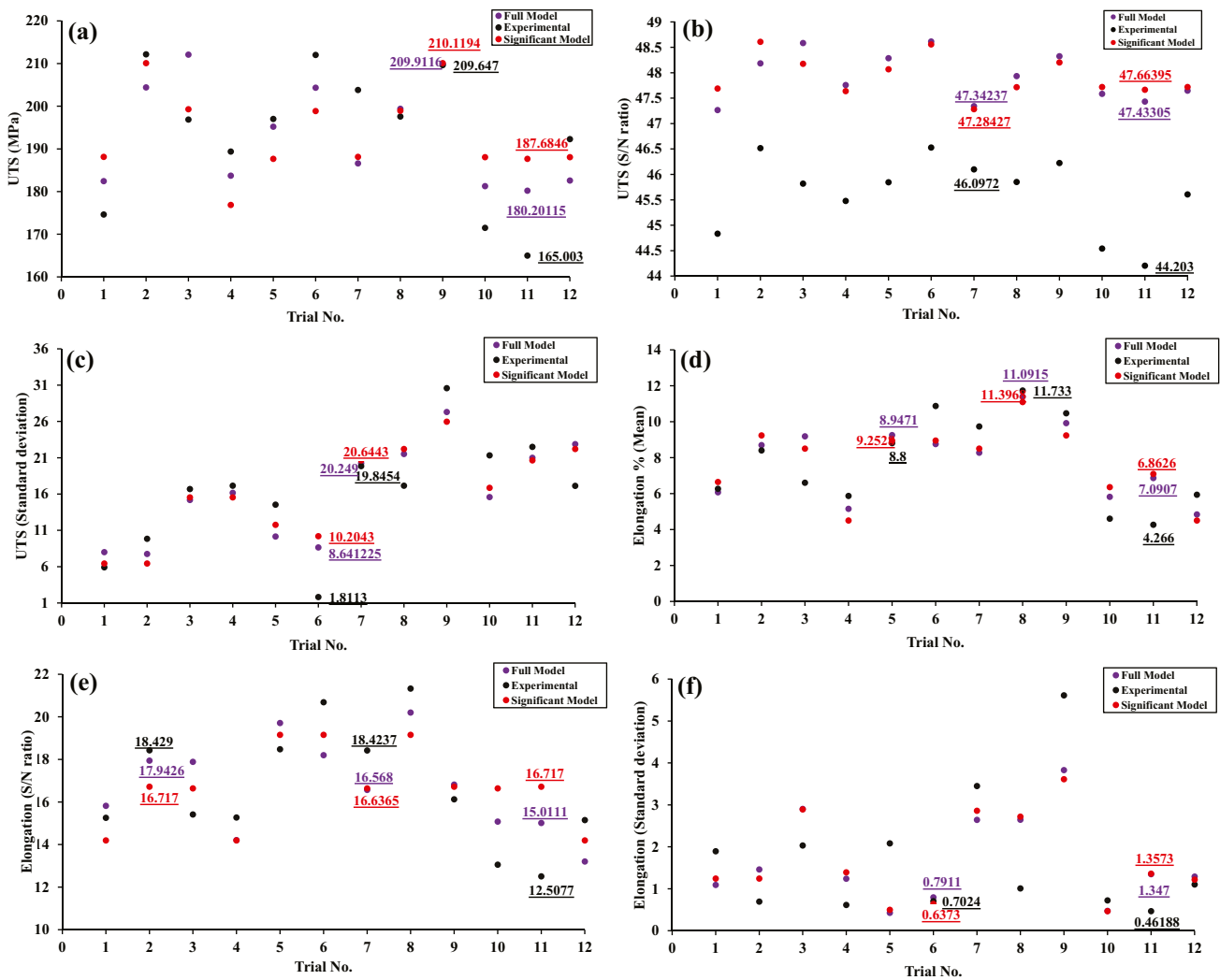
Fig. 7 Distributions of the experimental vs. the predicted results of UTS (**a** mean, **b** S/N ratio, **c** SD) and elongation (**d** mean, **e** S/N ratio, **f** SD)

and elongation. The most contributing parameters on tensile strength are traverse speed, plunge depth, and location of base metal with the percentage of 13.66, 13.47, and 12.57, respectively. As seen in Fig. 8, the values extracted from the surface plots of three different combinations are extremely

very close because the parameters have approximately the same contributions. No one of them dominates the other. It should control all three parameters. The RSM contour represents the boundary of tensile values, which range between the four dots. In all three surfaces, the contours start

Table 3 The accuracies of the full and significant models built based on L12OA

| | | Model accuracy % | | |
| | | L12OA | | L16OA [38] |
		Full model	Significant model	Significant model
UTS (MPa)	Mean	95.59	94.86	97.68
	S/N ratio	94.98	94.95	99.56
	Standard deviation	51.37	45.89	58.67
Elongation %	Mean	82.37	79.52	93.56
	S/N ratio	90.33	88.90	97.32
	Standard deviation	29.04	30.70	50.00
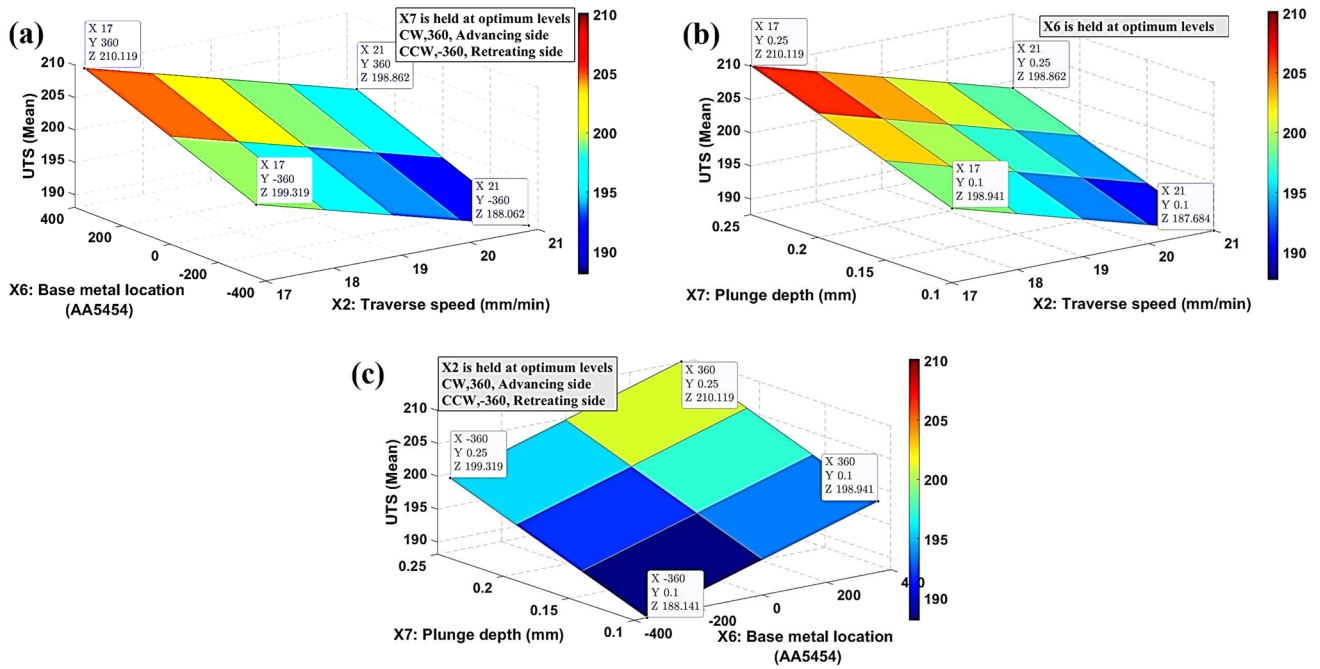
Fig. 8 Surface plots of the effect of the significant parameters on mean-UTS: **a** traverse speed/base metal location, **b** traverse speed/plunge depth, and **c** plunge depth/base metal location

from ~ 187–188 MPa and finish to ~ 210 MPa. It is noticed that by raising levels of parameters (i.e., plunge depth and metal location based on tool rotation direction), the tensile strength improves and advances to the maximum at high levels of both parameters. In contrast, by decreasing the traverse speed with increasing plunge depth or changing the AA545 side from RS to AS, the UTS increases.

For S/N ratio-UTS, as shown in Fig. 9, the rotational speed is added to the most contributing parameters with the parameters of mean-UTS. In all six surfaces, representing the effects of the four parameters, the contours start from ~47.68 and finish at ~48.68. The big difference of S/N ratios on all surfaces is about one. To make the UTS insensitive to noises, it should control these parameters. The S/N ratio increases by the effect of any two combinations of decreasing rotational speed, decreasing traverse speed, increasing plunge depth, and changing the location of AA5454 based on the tool rotation direction.

The most contributing parameters on elongation are traverse speed, pin profile, and the location of base metal with the percentage of 19.48, 14.58, and 28.39, respectively. In all three surfaces, as shown in Fig. 10a–c, the contours start from ~6.644% and finish at ~11.09%. Lessening the traverse speed with increasing the pin taper angle (pin profile) or changing the location of AA5454 from RS to AS, the elongation improves. For the S/N ratio (Fig. 10d), it may control

only the pin profile and location of the base metal. They contribute by 20.83% and 21.82, respectively.

3.1.4 Comparison between L12OA and L16OA

Some aspects may lead to a change in the contribution percentages of the parameters on the responses, and therefore the degree of their significance may change, and among these characteristics:

- Each array contains various combinations of the levels of the selected parameters during each experiment. Thus, different results appeared for each combination. In L12OA, each level is changed in six different combinations, while in L16OA, each level is changed in eight combinations.
- Using high fraction arrays can lead to a difference in output results and less accuracy.
- The results exhibited that the main effects of the levels for each parameter are very close. It is due to using a narrow domain, so-called tightening.
- Tightening, selecting numerous parameters, and performing fewer experiments reduce the accuracy of determining the main effects. Also, it leads to switching some of the optimum levels.
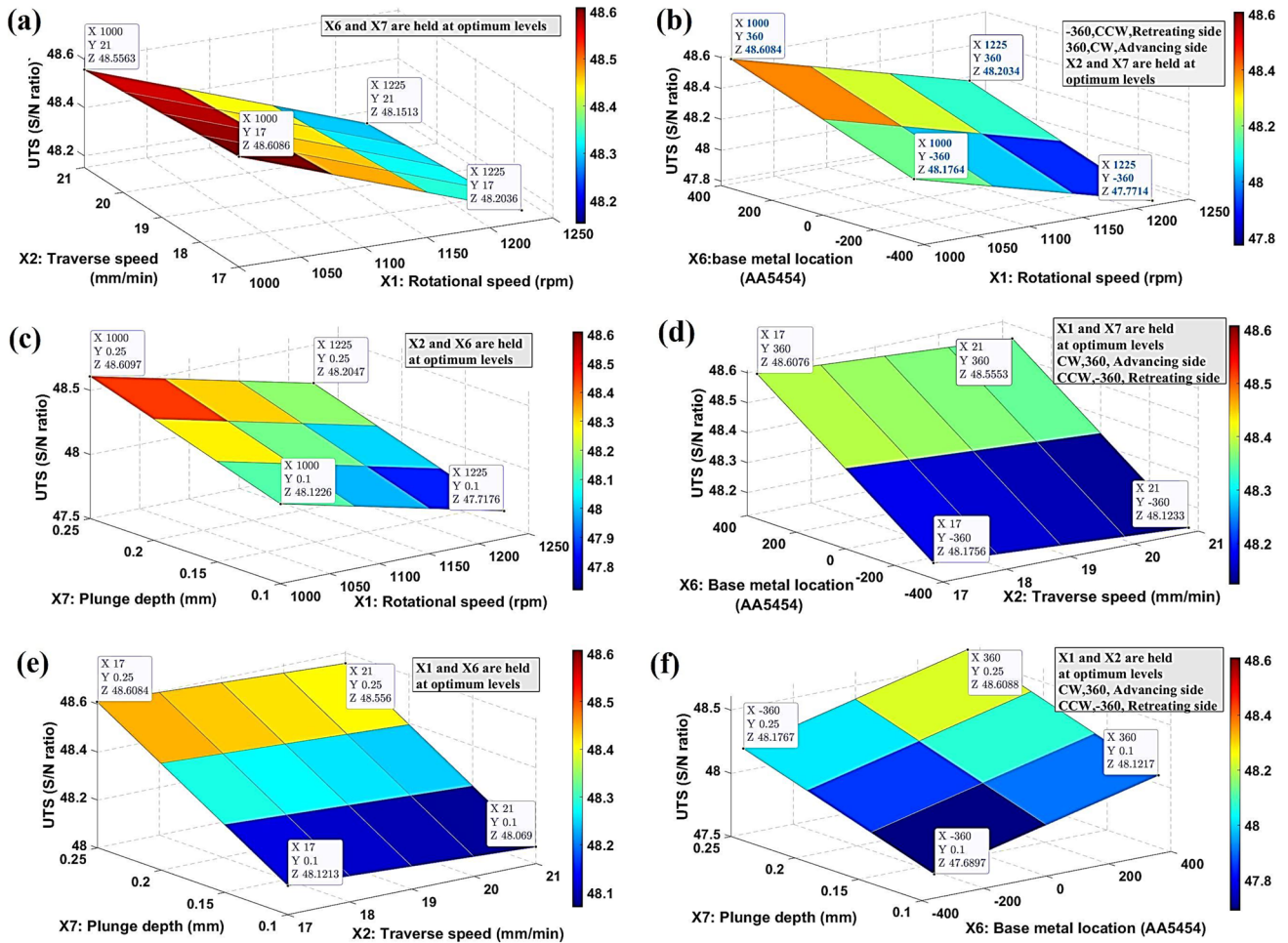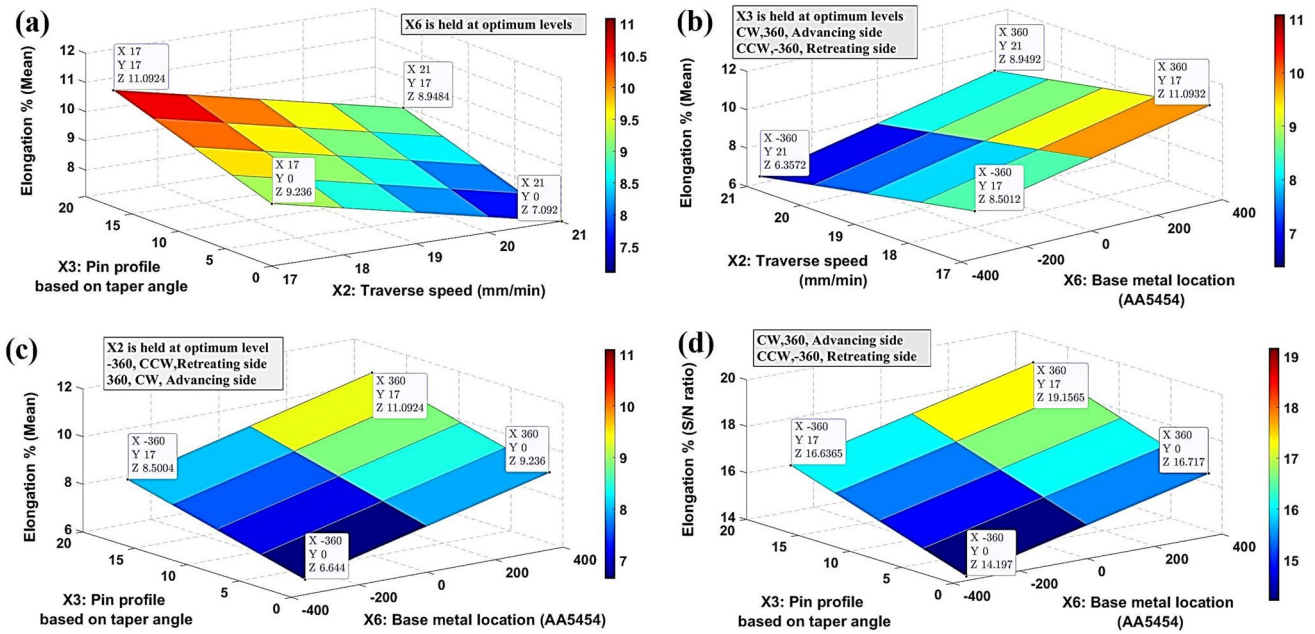
Fig. 9 Surface plots of the effect of the significant parameters on S/N ratio-UTS: **a** rotational speed/traverse speed, **b** rotational speed/base metal location, **c** rotational speed/plunge depth, **d** traverse speed/base metal location, **e** traverse speed/plunge depth, and **f** plunge depth/base metal location

Tables 4 and 5 illustrate the contribution percentages of the parameters based on L12OA and L16OA [38] on UTS and elongation, respectively. Travers speed still dominates the contribution in determining the UTS (mean and S/N ratio). It has the highest rank on both arrays. However, the rank of other parameters changed. In contrast, with standard deviation, welding speeds dominate the UTS with a ranking swap. For elongation, the rank of all parameters changed. D/d ratio dominates based on L16OA, while the location of base metal monopolizes based on L12OA. Table 6 gives the optimum levels of the process parameters for both arrays. Based on L16OA [38], the optimum levels are being consistent for the mean and S/N ratio of UTS except for the levels of pin profile. In addition to the pin profile, the tilt angle is inconsistent for the mean and S/N ratio of elongation. Based on L12OA, the optimum levels are consistent for all aspects

of UTS and elongation except for the D/d ratio and plunge depth on the S/N ratio of elongation. From both arrays, only the level of the base metal location is identical for all components of the responses. Also, there are some similarities and differences in levels for optimal results. The interactions between parameters added to the mathematical models for L16OA's models[38] increase the accuracy of models compared to the accuracy of the L12OA's models. As previously mentioned, the accuracies of the models are given in Table 3. As shown in Table 7, the deviations between the experimental and predicted results of the optimal joints based on L16OA are relatively small compared to the deviations obtained from L12OA.

The optimization of seven parameters using L16OA is more accurate than those using L12OA. It can summarize this in two characteristics:

Fig. 10 Surface plots of the effect of the significant parameters on mean-elongation: **a** traverse speed/pin profile, **b** traverse speed/base metal location, **c** pin profile/ base metal location, and **d** for S/N ratio

- The statistical errors obtained from L16OA are very small compared to the errors obtained from L12OA due to the addition of interactions. It represents the accuracy of selecting the proper array.
- The accuracies of the L16OA models are remarkably higher than the accuracies of the L12OA models. It accurately helps to predict the outputs by a less deviation from actual results.

Tightening leads to switching some of the optimum levels between both arrays. For UTS, both optimum levels obtained from L16OA (221 MPa) and L12OA (220 MPa) approximately provide the same results. For elongation %, the optimum levels obtained according to L12OA give the highest elongation, about 12.3%.

Table 4 The ranking of the FSW parameters optimized on UTS based on Taguchi L12OA and L16OA

Parameters	Rank											
	Mean				S/N ratio				Standard deviation			
	L12OA		L16OA [38]		L12OA		L16OA [38]		L12OA		L16OA [38]	
	Rank	%	Rank	%	Rank	%	Rank	%	Rank	%	Rank	%
Rotational speed	5	5.34	3*	9.08	4	8.37	3*	9.66	*1**	*50.83*	5	1.217
Traverse speed	*1*	*13.66*	1*	16.93	1	13.26	1*	18.58	5	0.38	1*	*34.363*
Pin profile	6	3.8	**7**	**0.11**	6	4.43	**7**	**0.01**	4	1.82	2*	12.312
D/d ratio	**7**	**2.97**	2*	12.47	**7**	**1.78**	2*	12.70	3	6.56	**7**	**0**
Tilt angle	4	5.69	6	2.09	5	5.96	6	1.58	2	13.13	3	6.156
Location of base metal	3	12.57	5	2.31	3	10.6	5	3.10	6	0	4	1.946
Plunge depth	2	13.47	4*	6.91	2	11.48	4*	7.71	**7**	**0**	6	0.633
Interactions		-		48.73		-		48.79		-		19.34
Error		42.33		0.78		44.14		1.347		27.23		24

Italics (highest); bold (lowest)

*Statistically significant

Table 5 The ranking of the FSW parameters optimized on elongation based on Taguchi L12OA and L16OA

Parameters	Rank											
	Mean				S/N ratio				Standard deviation			
	L12OA		L16OA [38]		L12OA		L16OA [38]		L12OA		L16OA [38]	
	Rank	%	Rank	%	Rank	%	Rank	%	Rank	%	Rank	%
Rotational speed	6	0	6	0.12	4	4.68	5	0.527	4	6.25	3*	8.041
Traverse speed	2*	19.48	3*	10.31	3	9.39	3*	9.534	1*	26.84	**7**	**0.005**
Pin profile	3	14.58	5	0.66	2	20.83	**7**	**0.164**	7	0.05	2*	14.6
D/d ratio	5	0.5	1*	21.43	6	1.04	1*	22.40	2	9.56	6	1.086
Tilt angle	4	3.26	**7**	**0.04**	5	1.13	6	0.223	3	6.77	4*	7.72
Location of base metal	1*	28.39	4	2.74	1*	21.82	4	2.894	6	0.19	5	6.972
Plunge depth	**7**	**0**	2*	15.96	**7**	**0.56**	2*	14.14	5	0.61	1*	16.45
Interactions		-		36.76		-		36.71		-		29.44
Error		33.77		11.7		40.56		12.09		49.73		11

Italics (highest); bold (lowest)

*Statistically significant

3.1.5 Critique of methodology

The experimental design selected for this investigation can be critiqued as follows:

- L12OA is employed to optimize seven parameters at two levels. This results in twelve trials which are approximately 1/10 of the experiments needed for full factorial. The L12OA was not designed to study the interactions between parameters. Statistical errors based on the ANOVA are significantly high on both responses. This is likely due to several reasons, such as inappropriate orthogonal array (i.e., high fraction), ignoring interactions, and ignoring other parameters. We recommend using the following array in the two-level table after L12/L16 OAs (i.e., L32OA (2^{31})). This array allows the studying of up to 31 objects between parameters and interactions.

- It ought to recognize noise parameters of FSW and then be optimized using Taguchi outer array.

- The technique carried out permits maximization of tensile strength and elongation one at a time based on the constraints of DOE in optimizing multi-responses. Fortunately, based on the results, the optimization of both outputs had the same levels. If we need to add other weld criteria such as yield strength, hardness, and distortion, there is a demand for multi- optimization formulation of FSW.

Table 6 The optimum levels of FSW parameters obtained based on Taguchi L12OA and L16OA

Optimum levels		L12OA	L16OA Ref. [38]
UTS (MPa)	Mean	$X_{11}, X_{21}, X_{32}, X_{42}, X_{52}, X_{62}, X_{72}$	$X_{12}, X_{22}, X_{32}, X_{41}, X_{52}, X_{62}, X_{71}$
	S/N ratio	$X_{11}, X_{21}, X_{32}, X_{42}, X_{52}, X_{62}, X_{72}$	$X_{12}, X_{22}, X_{31}, X_{41}, X_{52}, X_{62}, X_{71}$
Elongation %	Mean	$X_{11}, X_{21}, X_{32}, X_{42}, X_{52}, X_{62}, X_{72}$	$X_{12}, X_{22}, X_{31}, X_{41}, X_{51}, X_{62}, X_{71}$
	S/N ratio	$X_{11}, X_{21}, X_{32}, \mathbf{X_{41}}, X_{52}, X_{62}, \mathbf{X_{71}}$	$X_{12}, X_{22}, X_{31}, X_{41}, X_{51}, X_{62}, X_{71}$

Bold: level switching on L12OA.

Table 7 The deviations between the experimental and predicted results of the optimal joints based on L16OA and L12OA

		Experimental	Prediction (full model)	Deviation %	Prediction (significant model)	Deviation %
UTS (MPa)	L12OA	221.85, 209.17, 229 = 220.006 MPa	222.901	1.316	210	4.55
	L16OA	221.03 MPa			217.263	1.75
Elongation %	L12OA	12.4, 11.6, 13 = 12.3%	11.7741	4.275	11.092	9.82
	L16OA	10.83%			9.855	8.8

- The low difference in the main effects of parameter levels indicates using tight levels. It should extend the range between levels.
- Most investigations indicated that the modeling of FSW is nonlinear. So, even when they allow quantitative analysis, a linear model is often insufficient. One has to incorporate the nonlinearities in the model. This higher realism is the main advantage of nonlinear models, and not only in optimization. The prominent problem when studying the nonlinearity of most FSW parameters is the massive number of experiments required. To include the nonlinearity, it should use a nonlinear array with at least three levels. The proper array for this investigation is L81OA with 1/27 of full factorial design, but it is a costly and time-consuming process. Two levels of each parameter are not sufficient to study the nonlinear nature of the FSW process. Since the goal is to study the effect of selecting the arrays on contribution percentage (significance) and optimum levels, linear or nonlinear effects are not the major concern. Linear modeling is a special case of nonlinear where the objective function and constraints are linear.

3.2 Tensile properties

To optimize the process of joining dissimilar aluminum alloys, it must select responses (properties) used to evaluate the joints. Tensile properties are the most exceedingly employed. By estimating the force needed to elongate a specimen to failure, properties can be specified which will permit a developer to expect how a joint will act in its intentional applications. From this examination, it can recognize the greatest amount of stress that a joint can resist. UTS is considered during material forming and processing so that the material is in the flow regime and does not cross the necking point. Elongation is one of the most properties used

in metal forming, such as rolling, drawing, and extrusion. This tailor joint may be used in many applications that need formations before finishing.
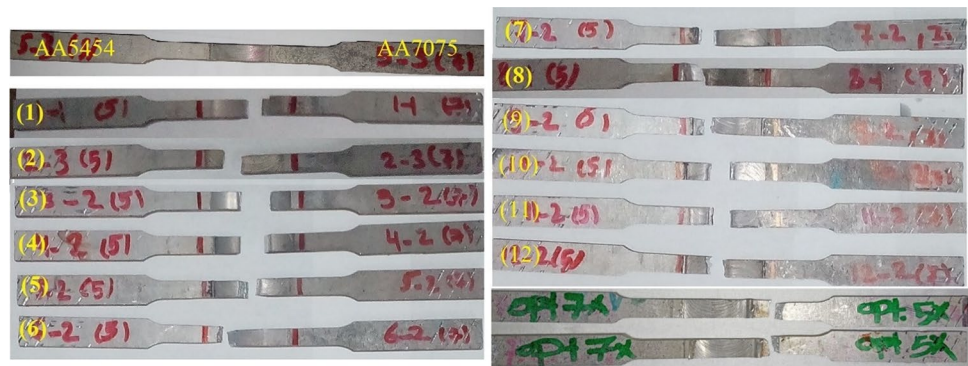
The UTS of the joints made by FSW is mainly affected by the formation of the stirring processing zone. The quality of the stirring zone depends on the efficiency of the combination of the selected process parameters [5]. Also, the UTS of the FSW joint is affected by the frictional heat generated in the weld zone and the area near the weld zone. It is normal in FSW that the material to be welded may lose some of its mechanical properties due to the effect of the frictional welding heat, especially if the material has a high strengthening temper between heat treatment and strain hardening. When welding dissimilar metals with a wide difference in the mechanical properties (as strength), the loss of the joint strength depends on the condition (temper) of the softer metal used in the dissimilar joints and if it will affect by the frictional heat [5]. Thus, the process parameters ought to be at optimal levels to accomplish high-quality joints.

The optimal welding efficiency did not reach 100% of the strength of the softer side. The joints' strengths were less than the strength of AA5454. Stress–strain curves of the base metals and optimal joint are given in Fig. 11. Before fracture, the optimal joint had a good plastic deformation with the highest strength and elongation [31]. The optimum strength was estimated to be 220 MPa, which the joint efficiency was 84.6% compared to the strength of the softer side (AA5454). The optimum elongation was calculated to be 12%, which was particularly higher than the elongations of both alloys. The elongation is higher about 300% of AA5454 and about 120% of AA7075. The metals used have different elongations based on their properties: AA5454-4% and AA7075-10%. In AA7075, the inferior strength of the joints compared to the corresponding base metals can be due to the microstructure modifications and the precipitates' state [44]. In addition, the precipitates overaged at the nugget and its

Fig. 11 Stress–strain curve of base metals and FSW optimal joint

AA7075-BM; 402MPa, 10%

AA5454-BM; 260MPa, 4%

Opt. Weld: UTS; 220.006 MPa (SD:10.04), E% ; 12.33% (SD:0.7023)
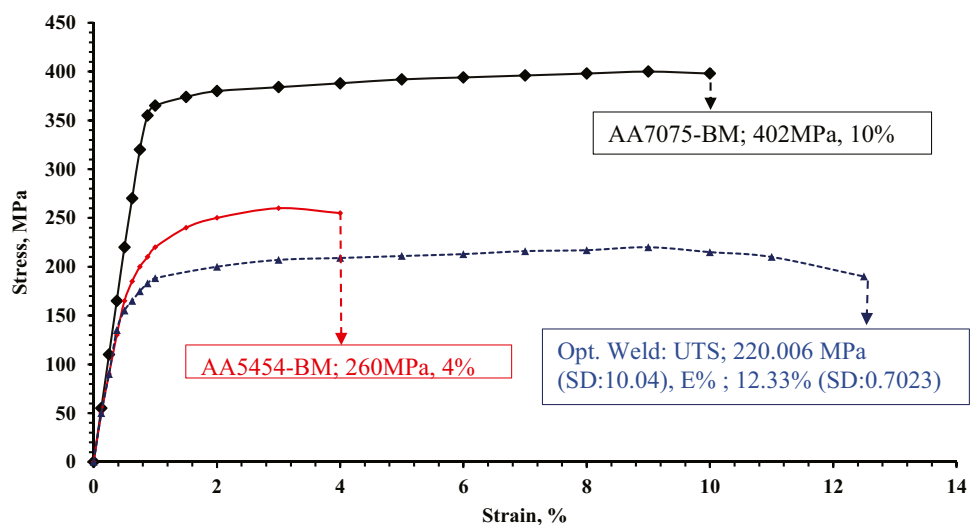
Fig. 12 The tensile fracture of the joints based on L12OA

vicinity (TMAZ/HAZ) will deteriorate the matrix strength [58]. As mentioned earlier, the AA7075 is not responsible for tensile failure of the dissimilar AA5454/AA7075. The welds obtained from L12OA with the optimum revealed a drop in UTS relative to the AA5454, to a level approximately within 36.43% and 15.4%. In addition to the stirring quality on the weld zone, the AA5454 side exhibited a pronounced softening to the base metal in the HAZ. This softening is due to annealing resulting from frictional heat, which relatively releases the strength provided by strain hardening. This material was rolled twice from 14 to 7 mm and then from 7 to 3.5 mm. Lang et al. [59] and Ditzel [60] reported the same results about UTS of similar or dissimilar joints with AA5454. They reported that the lowest drops in the UTS are 10.2% [59] and 15% [60]. The softening effect in the AA5454 side increases the elongation on this side. Also, Lang et al. [59] mentioned that the elongation of AA5454-H22 FSW welds increased from 7 to 18%, about 250%.

The basic qualification rule of dissimilar joining is that the fracture should appear on the softer side away from the weld zones. The present study did not satisfy this provision, with all joints failing in all three weld zones: nugget, TMAZ, and HAZ in the AA5454. The fracture locations usually occur in two regions, the weld zones and HAZ. The fracture occurs in the weld zone due to defects or poor stirring, while it turns to HAZ (lowest hardness site) in defect-free joints [28]. The fractures that occurred at the end of the weld face happened near the WZ/TMAZ interface due to the distinctive structure of both zones. TMAZ exhibits coarse-bent grains, while WZ consists of fine-equiaxed grains [19]. Annealing consequences in the HAZ result in the collapse of the strain hardening effects (by rolling work) [1]. As shown in Fig. 12, the tensile fracture lines (TFLs) occur at different regions due to various stirring based on different combinations of parameters. In trails 1, 3, 4, 5, 10, 11, and 12 from L12OA, TFLs were at the center of the weld zone. It reverts to poor stirring and unsuitable parameter combinations resulting in relatively low strengths. In trails 2, 6, 7, 8, and 9, TFLs are remarkably towards the end of weld width on the AA5454, whether its location is on advancing or retreating sides. The fracture locations are probable between the weld zone and TMAZ [27]. The optimum joint failed at the HAZ. For all joints, as shown in Fig. 13, the tensile fractures that occurred in HAZ (a), near to center (b), or TMAZ/WZ (c) show a typical shear mode at an angle of 45°. The fracture angle of 45° was also reported [57].

3.3 Surface morphology

A photograph of the weld face and the weld root of the welded joints according to the L12OA is given in Fig. 14. The shape of the weld face and the weld root depends on the parameters used to produce the joint. All the upper surfaces of the joints were smooth without visible defects such as tunnels and cracks and with a periodical semicircular band (tool markers) depending on the shoulder features and rotational stirring. Regardless, the smoothness relatively declined with a minimum flash observed in some areas or joints (6, 7, 8, and 9), inducing a thinning begun from toes through to the interface. The flash considers as metal loss from base metal at each side due to either higher tool plunging, or high heat input produced by a condition of both speeds. The axial force, an uncontrollable parameter, also contributed to the formation of flash [45]. The plasticized material experienced too much turbulence due to high heat input that permitted the stirred metals to escape to the upper surface resulting in an excessive flash in joints 7,

Fig. 13 A typical shear mode of the joints at **a** HAZ, **b** near to the center, and **c** TMAZ/WZ
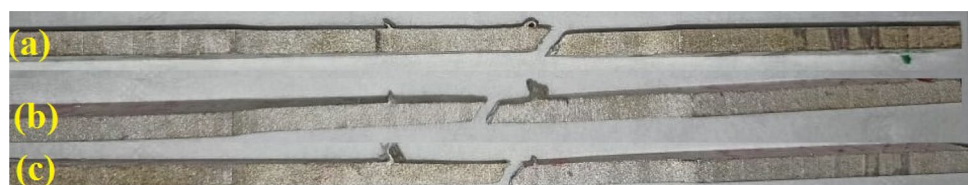
Fig. 14 Photograph of the weld face and the weld root of the joints according to L12OA

(1) (2) (3) (4) (5) (6)

(7) (8) (9) (10) (11) (12)
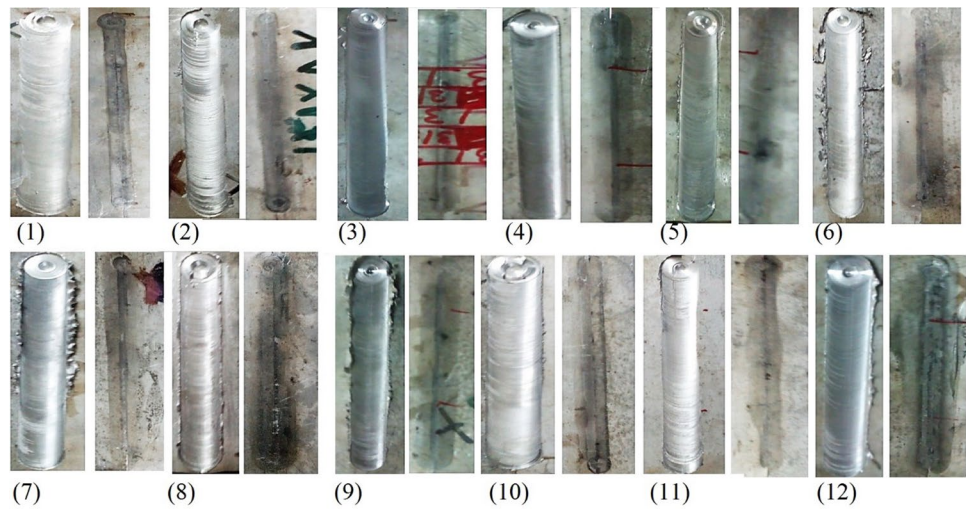
8, and 9 [58]. Mechanical performance may be influenced by the surface finish quality and flash formation [18]. The root sides did not stick with the backing plate during the operation. It means that the contact time based on traverse speed with plunge depth was suitable during all twelve joints.
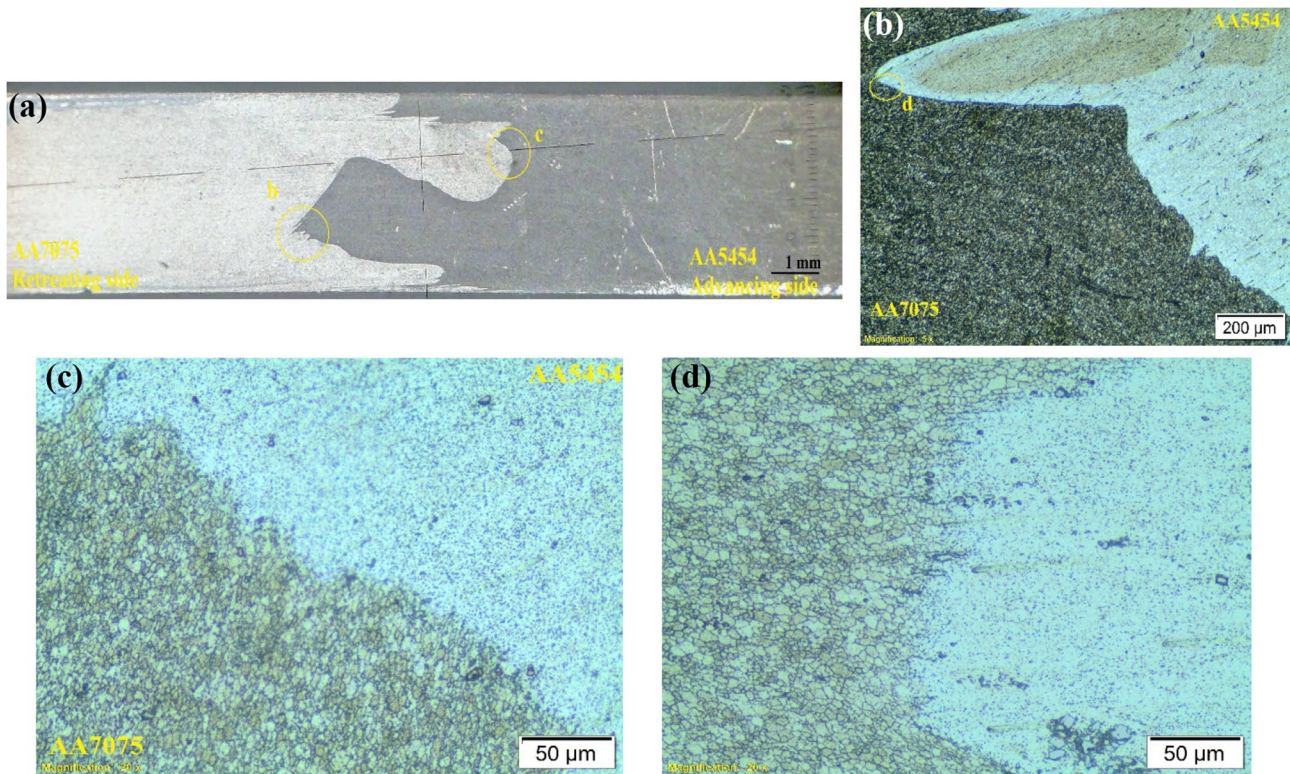
3.4 Microstructure

The microstructure of the base metals of the AA5454 and the AA7075 is shown in Fig. 15. The strain hardening effect is observed in the microstructure of the AA5454 (5XXX strain hardening alloy). The solubility extent of Mg in Al plays the meaningful control of the formation of $MgAl_2$ particles, which formed a banding along the rolling direction [19]. The grains of the AA7075 are very large and have an elongated pancake shape due to the hot rolling. Figure 16 a shows a macrograph of the transverse section of the lowest strength joint obtained from L12OA (T11) with sharp borders at the interface between both alloys. The presence of sharp borders acts as a component of discontinuity. The failure may ensue along with any sharp edges [18]. Figure 17 a shows a macrograph of the transverse section of the joint 8. The same stirring pattern was approximately created but

with different plasticized material volumes. This is due to the difference in shoulder and pin features and the D/d ratio. Both tapered (T8) and cylindrical (T11) profiles used show relatively poor intermixing. M. M. Hasan et al. [35] indicated similar observations. They also observed that the material flow improved when adding a chamfer to one side of the tapered pin [35, 61]. The stirring action was insufficient between both alloys, even with the presence of reasonably dynamic recrystallization, as shown in Figs. 16b–d and 17b, c. The interlocking bonding pattern of one big bulk of each metal into the other affected the quality of the joint [62]. The joint produced using the optimum levels exhibited the highest of both tensile strength and elongation, most probably due to a relatively good stirring and fine equiaxed grains of the weld zone as shown in Fig. 18. The macrostructure of this joint (Fig. 18a) shows more stirring between AA5454 and AA7075, and the metals were stirred with a small size compared to those in the first group. The stirring action became more effective compared to the other joints with showing stirring of alternating layers (Fig. 18b) and fragments (Fig. 18c). A complete stirring form of FSW is not observed in these joints due to the wide difference between both metals.

**Fig. 15** Optical micrograph of base metals **a** AA7075 and **b** AA5454

(a)   (b)

50 µm   50 µm
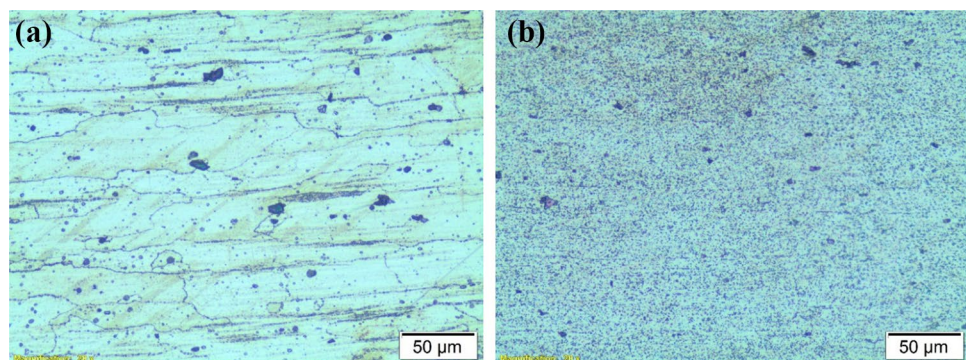
Fig. 16 Macrostructure of the lowest strength joint **a** with optical micrographs at the interface, **b** region b in a, **c** region c in a, and **d** region d in b

The depth and width of the stirring zone depend on the pin length and the D/d ratio, respectively. The 3.2 mm pin length was sufficient to stir up to 3.5 mm metal thickness. The width of the joints depends on the amount of heat input, stirring flow rate, and forging action by the characteristics of the tool profile. The boundary of the weld zone is to be in a location between the shoulder diameter and pin diameter. Depending on the heat input, the nugget width decreases with thickness. As seen in Figs. 15–18, the characteristics

of shoulder driven metal-flow region depend on which alloy was placed on the Advancing side, shoulder diameter, and shoulder feature. This region, in-width, with increasing shoulder diameter, was more saturated with the material placed in the AS. In contrast, the depth of these regions was more similar. The shoulder feature played the role of the metal profile in this area. The metal was more warp with the concave feature (as in T8), while metal tended to be sharp with the flat shoulder (as in T11) [62].

Fig. 17 Macrostructure of the joint 8 **a** with optical micrographs at the interface, **b** region b in a, and **c** region c in a
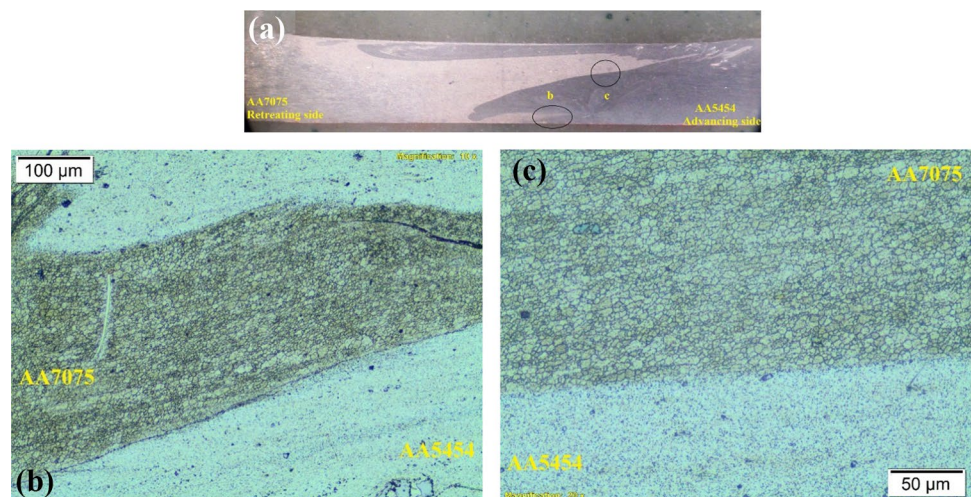
Fig. 18 Macrostructure of the optimal joint **a** with SEM micrographs at the interface, **b** region b in a, **c** region c in a, **d** region d in a, and **e** region e in b
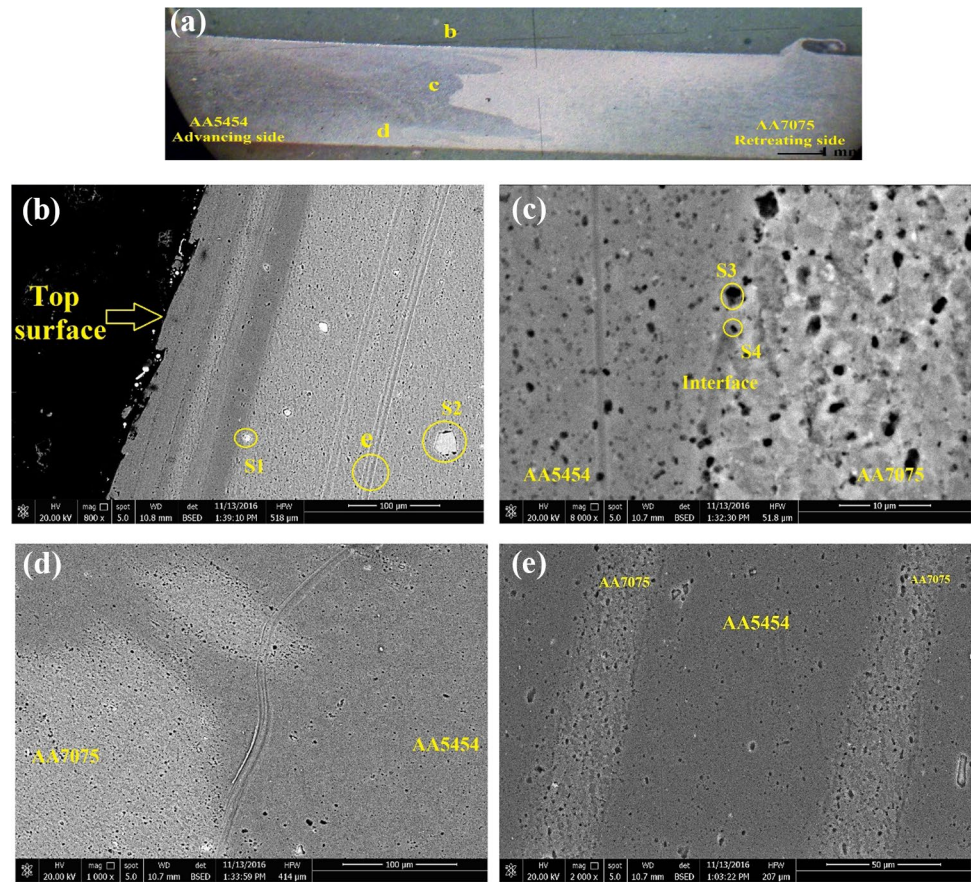

Figure 19 shows the EDS analysis with the allocation of the chemical elements. The results verify that the stirring zone was formed by both AA7075 and AA5454. The shiny S1 particle (Fig. 18b), at the interface of alternating layers of both alloys under the shoulder, is rich in Al, Fe, Mn, Si, and Mg with the wt. % of 72.7, 12.15, 7.95, 3.57, and 1.23, respectively. Therefore, the shiny particle is attributed to the α-AlFeMnSi intermetallic. This is consistent with the result noted by Wei et al. [63]. The S2 particle (Fig. 18b) is rich in Al, Mg, C, Zn, Ti, Cr, Cu, V, Ca, and Mn with the wt. % of 68.68, 7.27, 5.55, 5.47, 4.97, 4.4, 1.5, 1.04, 0.8, and 0.32, respectively. The composition is consistent with the chemical composition of AA7075 and some elements (i.e., C, V, Ca) from H13-tool steel used. These elements indicate that the tool suffered from wearing during the process. The wt. % of the dark particles S3 and S4 at the interface in the weld zone (Fig. 18c) are 1.59 Mg, 89.1 Al, 3.28 Zn, and 2.75 Mg, 76.6 Al, and 4.05 Zn, respectively. They refer to the main intermetallic particles from AA7075, $MgZn_2$. Kalemba et al. [64] reported that the sire zone of dissimilar joints between AA7075 and AA5083 held some phases related to both alloys (i.e., Al_7Cu_2Fe, $MgZn_2$ from AA7075, and Mg_2Si from AA5083). This study reveals that FSW acceptably can assemble joints between AA5454 and AA7075, presenting the proficiency of FSW with welding

of dissimilar alloys. Though, the microstructures exhibit a shortage of effective intermixing [1]. Similar stirring actions (i.e., insufficient mixing, chaotic mixing, and alternating layers) were also reported with different combinations of aluminum alloys [65–67].

3.5 Fractography

One of the aims of fractographic examination is to determine the cause of a failure by studying the characteristics of a fractured surface and knowing the origin of cracking. It helps to predict the outcome of the process. The tensile fracture of the optimum joint happened at the HAZ on the AA5454 side with approximately 45° along the tensile axis. Figure 20a and b show the fracture surface of the AA5454 base metal and the optimum joint. Both the fracture surfaces show necking plastic deformation (ductile mode). In the fracture surface of the AA5454 base metal, the dimples are a little deeper and smaller than those in the optimum joint. Figure 20 c shows SEM images of the fracture surface towards the bottom region of the weld. In this area, there are three different modes of failure observed, which are (1) the normal ductile mode with sheared dimples, (2) intergranular brittle fracture surface, and (3) severe brittle surface. The observation of the different failure modes on the fracture surface demonstrates that this area
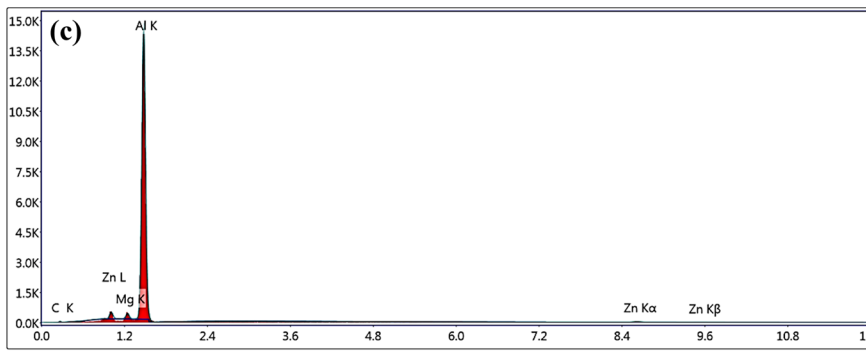
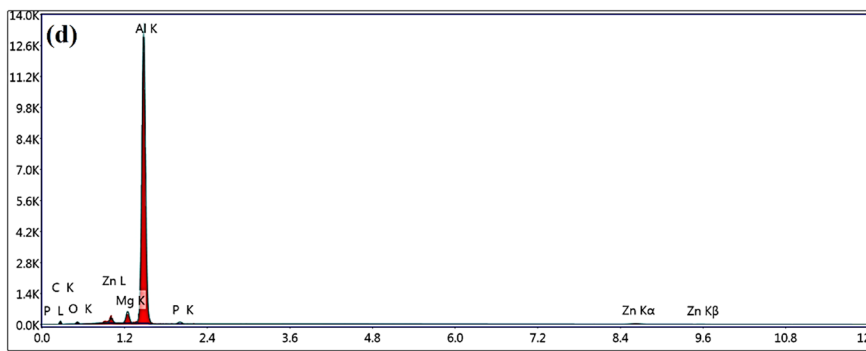| KV: 20 | Mag: 2000 | Takeoff: 34 | Live Time(s):30 | Amp Time (µs): 7.68 | Resolution: (eV)122.8 |

(a) S1
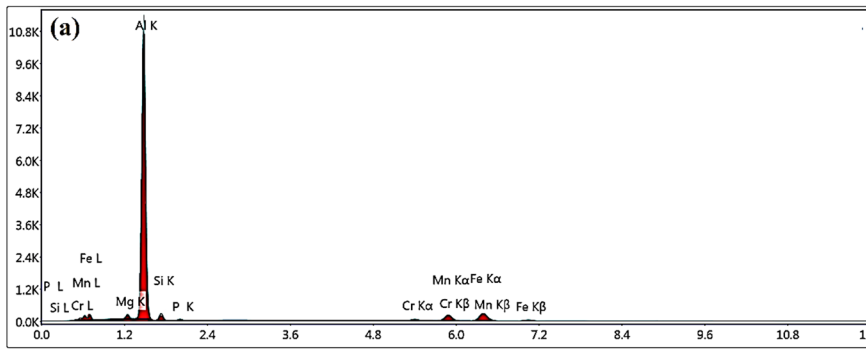
Element	Weight %	Atomic %
Mg K	1.23	1.54
Al K	72.7	81.91
Si K	3.57	3.86
Mn K	7.95	4.4
Fe K	12.15	6.61

(b) S2
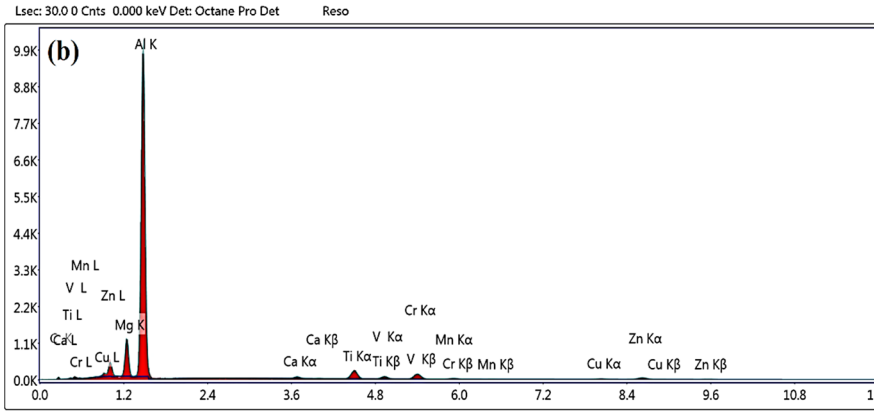
Element	Weight %	Atomic %
Mg K	7.27	8.19
Al K	68.68	69.77
Zn K	5.47	2.29
Mn K	0.32	0.16
Cu K	1.5	0.65
Ti K	4.97	2.85
Ca K	0.8	0.55
V K	1.04	0.56
C K	5.55	12.67
Cr k	4.4	2.32

(c) S3

Element	Weight %	Atomic %
Mg K	1.59	1.67
Al K	89.1	84.23
Zn K	3.28	1.28

(d) S4

Element	Weight %	Atomic %
Mg K	2.75	2.63
Al K	76.6	66.2
Zn K	4.05	1.44

Fig. 19 EDS analysis with the allocation of the chemical elements of particles formed: (**a**) S1, (**b**) S2, (**c**) S3, and (**d**) S4 (spots 1–4 from Fig. 18**b, c**)

Fig. 20 SEM images of the fracture surfaces: **a** AA5454 base metal, **b** HAZ-optimum joint, and **c** at the lower region of the weld (1 and 2 enlarged SEM of the regions 1 and 2 in **c**)
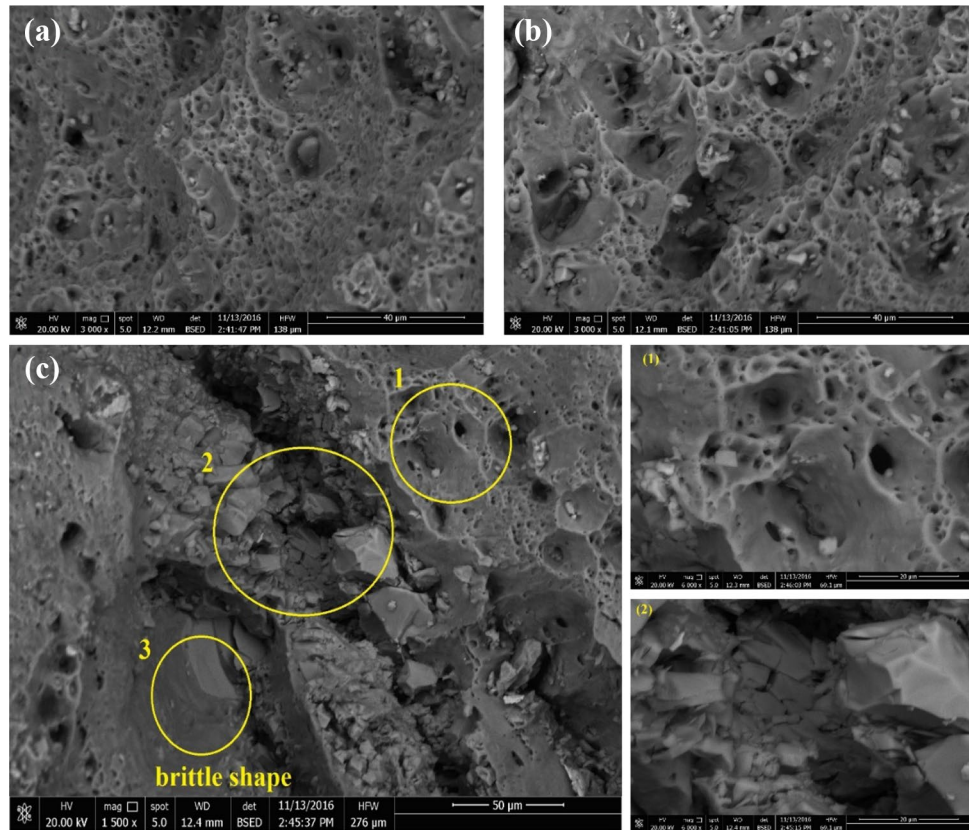
was located between different weld zones (HAZ/TMAZ), as in ref. [68]. The deep dimples relate to the start of the crack. After the initial phase of crack formation, the specimen experiences overloading, and the dimples are sheared. In the brittle areas, crack often propagates by cleavage—breaking of atomic bonds along specific crystallographic planes (cleavage planes). Ductile objects absorb energy before failure, so there are intrinsically safer than brittle objects.

4 Conclusions

In this study, a statistical optimization based on experimental work was conducted to consider ultimate tensile strength (UTS) and elongation of dissimilar joints between AA5454 and AA7075 by friction stir weld (FSW). Taguchi L12 orthogonal array, a fractional-factorial design, was used to arrange seven parameters of FSW at two levels. The parameters considered are rotational speed (RS), traverse speed (TS), pin profile(PP), the ratio between shoulder diameter and pin diameter (D/d ratio), tilt angle (TA), plunge depth (PD), and location of base metal (LBM). Mathematical models for responses were developed using response surface methodology to correlate the significant parameters. Analysis of variance (ANOVA) was employed to obtain the main effects and the degree of significance of each parameter

on the responses. Moreover, the investigation explored the microstructure and fractography of dissimilar joints and base metals by using optical and scanning electron (SEM) microscopes. The main novelty of this work is to develop a comparative study of the optimization of FSW parameters using different orthogonal arrays. The comparisons were between the results of this research using Taguchi L12OA and the results of the Abd Elnabi et al. [38] using Taguchi L16OA. The investigation's results are summarized as follows:

- Based on L12OA, the results obtained for UTS and elongation are within (165–212.2 MPa) and (4.3–11.7%), respectively. By comparison with AA5454-side, the joint efficiencies range from 63.5 to 81.6%, and the elongations range from 106.65 to 293.33%.
- Using plunge depth without force controller might produce relatively different weld qualities at the same operation leading to a slightly high standard deviation.
- The main effects of the levels for each parameter are very close that demonstrates using a narrow domain.
- According to the ANOVA results, all the considered parameters are insignificant at any of 90%, 95%, or 99% confidence levels (C.Ls.) on elongation for S/N ratio, standard deviation (SD), and the mean. Also, all the parameters are insignificant at any of 95% or 99% C.Ls. on UTS for all except for the rotational speed on SD (90% C.L.).

- TS, PD, and LBM are the most contributing parameters on UTS by 13.66%, 13.47%, and 12.57% for mean and 13.26%, 11.48%, and 10.6% for S/N ratio, respectively. Also, the most contributing parameters on SD-UTS are RS, D/d ratio, and TA by 50.83%, 6.56%, and 4.96%, respectively.
- LBM, TS, and PP are the most contributing parameters on elongation by 28.39%, 19.48%, and 14.58% for mean and 21.82%, 9.39%, and 20.83% for S/N ratio, respectively. Also, the most contributing parameters on SD-elongation are TS, D/d ratio, RS, and TA by 26.84%, 9.56%, 6.77%, and 6.25%, respectively.
- The optimal levels obtained to maximize the UTS and elongation are similar for the mean and S/N ratio except for two levels in the S/N ratio of elongation. The optimum joint was produced using the levels of 1000 rpm (RS), 17 mm/min (TS), 2° (TA), 0.25 mm (PD), 3 $D_{shoulder}/d_{pin}$ ratio, tapered pin profile, and AA5454 placed on the advancing side. The confirmation experiments were carried out, and the average values of the UTS and elongation were 220.006 MPa (S/N ratio of 46.83) and 12.3% (S/N ratio of 21.793), respectively.
- The expected responses have good and relatively high agreements compared with the experimental results. The accuracies of models of both UTS and elongation based on the mean and S/N ratio are relatively high (between ~ 80 and ~ 96%), and very low on SD (between ~ 29 and ~ 51%).
- All the upper surfaces of the joints were smooth (except for T6, 7, 8, and 9) without visible defects such as tunnels and cracks, and with a periodical semicircular band. The uncontrollable axial force and/or too much turbulence of the plasticized metals due to high heat input contributed to the formation of flash in T6–T9.
- The tensile fractures occurred in the weld zones (nugget/TMAZ) of poor stirring joints and HAZ-AA5454 of defect-free joints. Annealing effects in the HAZ resulted in the collapse of the strain hardening effects of the AA5454.

By comparison between L12OA and L16OA results:

1. Tightening, selecting numerous parameters, and performing fewer experiments (high fraction arrays) reduced the accuracy of determining the main effects. Also, it led to switching some of the optimum levels.
2. For UTS, TS dominated the contribution in determining the UTS (mean and S/N ratio), and the ranking of other parameters changed.
3. For elongation, the rank of all parameters changed. D/d ratio dominated based on L16OA, while the location of base metal monopolizes based on L12OA.
4. The interactions between parameters added to the mathematical models for L16OA's models increased the accuracy of models compared to the accuracy of the L12OA's models.

Despite the deficiency of effective intermixing, the study reveals that FSW acceptably can assemble joints between AA5454 and AA7075, presenting the proficiency of FSW with welding dissimilar aluminum alloys.

Appendix. Analysis of variance (ANOVA) for experimental results of the FSW process

Table 8 The experimental results of UTS and elongation based on the Taguchi array

Control parameters (L12-OA)								UTS (MPa)			Elongation %		
No	X1	X2	X3	X4	X5	X6	X7	Trial 1	Trial 2	Trial 3	Trial 1	Trial 2	Trial 3
1	1	1	1	1	1	1	1	173.60	169.30	181.0	5.6	4.8	8.4
2	1	1	1	1	1	2	2	206	207.04	223.54	8	8	9.2
3	1	1	2	2	2	1	2	205.48	177.65	207.52	7	4.4	8.4
4	1	2	1	2	2	1	1	173.57	207.61	187.03	6.4	6	5.2
5	1	2	2	1	2	2	1	190.02	213.73	187.29	7.6	11.2	7.6
6	1	2	2	2	1	2	2	210.50	214.03	211.56	11.6	10.2	10.8
7	2	1	2	2	1	1	1	181.30	218.72	211.47	6	12.8	10.4
8	2	1	2	1	2	2	1	194.76	182.04	216	10.8	11.6	12.8
9	2	1	1	2	2	2	2	222.41	231.79	174.74	13.4	14	4
10	2	2	2	1	1	1	2	188.24	147.48	178.78	4.4	4	5.4
11	2	2	1	2	1	2	1	190.94	150.60	153.47	4.8	4	4
12	2	2	1	1	2	1	2	205.61	172.96	198.32	7	4.8	6

Table 9 ANOVA table for UTS-S/N ratio

S/N by factor level		Degree of Freedom (DOF)	Sum of square (SS)	Mean square (V)	*F*-calculated *(pooled effect)		Percentage of contribution *P*%
1	2						
*X*1: Rotational speed (rpm)							
275.0171	272.521	1	0.5166	0.5166	0.76	Pooled	8.37%
*X*2: Traverse speed (mm/min)							
275.3392	272.1989	1	0.8185	0.8185	1.20	1.528	13.26%
*X*3: Pin profile (°)							
272.86	274.6781	1	0.2736	0.2736	0.40	Pooled	4.43%
*X*4: D/d ratio							
273.1917	274.3464	1	0.1099	0.1099	0.16	Pooled	1.78%
*X*5: Tilt angle (°)							
272.7161	274.822	1	0.3673	0.3673	0.54	Pooled	5.96%
*X*6: location of base metal							
272.371	275.1671	1	0.6544	0.6544	0.96	Pooled	10.60%
*X*7: Plunge depth (mm)							
272.3077	275.2304	1	0.7089	0.7089	1.04	Pooled	11.48%
Error		4/10*	2.7257/5.3565*	0.6814/0.5356*			44.14%/86.74%*
Total		11	6.1750				100%

*Pooled ANOVA after Pooling Insignificant Terms

Table 10 ANOVA table for UTS-mean

Mean by factor level		Degree of freedom (DOF)	Sum of square (SS)	Mean square (V)	*F*-calculated *(pooled effect)		Percentage of contribution *P*%
1	2						
*X*1: Rotational speed (rpm)							
1182.155	1139.877	1	147.84	147.84	0.50	Pooled	5.34%
*X*2: Traverse speed (mm/min)							
1194.786	1127.246	1	378.34	378.34	1.29	1.58	13.66%
*X*3: Pin profile (°)							
1143.176	1178.856	1	105.14	105.14	0.36	Pooled	3.80%
*X*4: D/d ratio							
1145.236	1176.796	1	82.16	82.16	0.28	Pooled	2.97%
*X*5: Tilt angle (°)							
1139.189	1182.843	1	157.64	157.64	0.54	Pooled	5.69%
*X*6: location of base metal							
1128.546	1193.486	1	353.17	353.17	1.20	Pooled	12.75%
*X*7: Plunge depth (mm)							
1127.482	1194.55	1	373.04	373.04	1.27	Pooled	13.47%
Error		4/10*	1172.68/2391.67*	293.17/239.16*			42.33%/57.48%*
Total		11	2770.01				100%

*Pooled ANOVA after Pooling Insignificant Terms

Table 11 ANOVA table for UTS-standard deviation

Standard deviation by factor level 1	2	Degree of freedom (DOF)	Sum of square (SS)	Mean square (V)	F-calculated *(pooled effect)		Percentage of contribution P%
X1: Rotational speed (rpm)							
65.9425	128.5729	1	328.156	328.156	5.749	10.35	50.85%
X2: Traverse speed (mm/min)							
100.0405	94.4749	1	2.470	2.470	0.04	Pooled	0.38%
X3: Pin profile (°)							
103.1395	91.3759	1	11.772	11.772	0.206	Pooled	1.82%
X4: D/d ratio							
76.0876	118.4278	1	42.330	42.330	0.74	Pooled	6.56%
X5: Tilt angle (°)							
81.2556	113.2598	1	32.0031	32.0031	0.560	Pooled	4.96%
X6: location of base metal							
98.066	96.4494	1	0.186	0.186	0	Pooled	0%
X7: Plunge depth (mm)							
97.1133	97.4021	1	0.002	0.002	0	Pooled	0%
Error		4/10*	228.314/317.158*	57.078/31.715*			35.38%/49.15%*
Total		11	645.314				100%

*Pooled ANOVA after Pooling Insignificant Terms

Table 12 ANOVA table for elongation-S/N ratio

S/N by factor level 1	2	Degree of freedom (DOF)	Sum of square (SS)	Mean square (V)	F-calculated *(pooled effect)		Percentage of contribution P%
X1: Rotational speed (rpm)							
103.5314	96.59319	1	4.0115	4.0115	0.46	Pooled	4.68%
X2: Traverse speed (mm/min)							
104.976	95.14816	1	8.0495	8.0495	0.93	Pooled	9.39%
X3: Pin profile (°)							
92.7419	107.3826	1	17.8625	17.862	2.05	3.267	20.83%
X4: D/d ratio							
101.696	98.4285	1	0.8897	0.8897	0.10	Pooled	1.04%
X5: Tilt angle (°)							
98.3577	101.7668	1	0.9685	0.9685	0.11	Pooled	1.13%
X6: location of base metal							
92.5701	107.5544	1	18.7108	18.710	2.15	3.423	21.82%
X7: Plunge depth (mm)							
101.258	98.86655	1	0.4766	0.4766	0.05	Pooled	0.56%
Error		4/9*	34.8001/49.196*	8.7002/5.466*			40.57%/57.35%*
Total		11	85.7693				100%

*Pooled ANOVA after Pooling Insignificant Terms

Table 13 ANOVA table for elongation-mean

Mean by factor level		Degree of freedom (DOF)	Sum of square (SS)	Mean square (V)	F-calculated *(pooled effect)		Percentage of contribution P%
1	2						
X1: Rotational speed (rpm)							
46.8	46.7333	1	0.0004	0.0004	0.00	Pooled	0.00%
X2: Traverse speed (mm/min)							
53.2	40.333	1	13.7959	13.7959	2.31	4.164	19.48%
X3: Pin profile (°)							
41.2	52.333	1	10.3293	10.3293	1.73	3.1178	14.58%
X4: D/d ratio							
45.7333	47.8	1	0.3559	0.3559	0.06	Pooled	0.50%
X5: Tilt angle (°)							
44.1333	49.40	1	2.3115	2.3115	0.39	Pooled	3.26%
X6: location of base metal (LM)							
39	54.5333	1	20.1070	20.1070	3.36	6.069	28.39%
X7: Plunge depth (mm)							
46.6667	46.8667	1	0.0033	0.0033	0.00	Pooled	0.00%
Error		4/8*	23.918/26.51*	5.9796/3.313*			33.77%/37.55%*
Total		11	70.8219				100%

*Pooled ANOVA after Pooling Insignificant Terms

Table 14 ANOVA table for elongation-standard deviation

Standard deviation by factor level		Degree of freedom (DOF)	Sum of square (SS)	Mean square (V)	F-calculated *(pooled effect)		Percentage of contribution P%
1	2						
X1: Rotational speed (rpm)							
8.004	12.3482	1	1.5751	1.5751	0.50	Pooled	6.25%
X2: Traverse speed (mm/min)							
14.6765	5.6763	1	6.7503	6.7503	2.16	3.814	26.84%
X3: Pin profile (°)							
10.3658	9.987	1	0.0120	0.0120	0.00	Pooled	0.05%
X4: D/d ratio							
6.7981	13.55486	1	2.4041	2.4041	0.77	1.3582	9.56%
X5: Tilt angle (°)							
7.9178	12.4357	1	1.7014	1.7014	0.54	Pooled	6.77%
X6: location of base metal (LM)							
9.80214	10.5505	1	0.0466	0.0466	0.01	Pooled	0.19%
X7: Plunge depth (mm)							
9.4969	10.8559	1	0.1539	0.1539	0.05	Pooled	0.61%
Error		4/9*	12.506/15.995*	3.126/1.77*			49.73%/60.72%*
Total		11	25.1466				100%

*Pooled ANOVA after Pooling Insignificant Terms

Table 15 F values for 90, 95, and 99% confidence levels

DOF$_{parameter}$ = 1 (2-level parameters)			
Confidence level %	90%	95%	99%
$F_{Tabulated}$			
DOF$_{Error}$ = 4	4.54	7.71	21.2
DOF$_{Error}$ = 7	3.59	5.59	12.2
DOF$_{Error}$ = 8	3.46	5.32	11.3
DOF$_{Error}$ = 9	3.36	5.12	10.6
DOF$_{Error}$ = 10	3.28	4.96	10

Declarations

References

1. Koilraj M, Sundareswaran V, Vijayan S, Koteswara Rao SR (2012) Friction stir welding of dissimilar aluminum alloys AA2219 to AA5083 – optimization of process parameters using Taguchi technique. Mater Des 42:1–7. https://doi.org/10.1016/j.matdes.2012.02.016

2. Kumar S, Kumar S (2015) Multi-response optimization of process parameters for friction stir welding of joining dissimilar Al alloys by gray relation analysis and Taguchi method. J Braz Soc Mech Sci Eng 37:665–674. https://doi.org/10.1007/s40430-014-0195-2

3. Bokov DO, Jawad MA, Suksatan W, Abdullah ME, Świerczyńska A, Fydrych D, Derazkola HA (2021) Effect of pin shape on thermal history of aluminum-steel friction stir welded joint: computational fluid dynamic modeling and validation. Materials 14(24):7883. https://doi.org/10.3390/ma14247883

4. Janeczek A, Tomków J, Fydrych D (2021) The influence of tool shape and process parameters on the mechanical properties of AW-3004 aluminium alloy friction stir welded joints. Materials14(12):3244. https://doi.org/10.3390/ma14123244

5. Mishra RS, Ma ZY (2005) Friction stir welding and processing. Mater Sci Eng R Rep 50(1–2):1–78. https://doi.org/10.1016/j.mser.2005.07.001

6. Abd Elnabi MM, Osman TA, El Mokadem AE (2018) Modeling and optimization of friction stir welding parameters for joining dissimilar aluminum alloys. Adv J Grad Res 4(1):1–14. https://doi.org/10.21467/ajgr.4.1.1-14

7. Abd Elnabi MM, Osman TA, El Mokadem A, Elshalakany AB (2017) Mechanical properties and macrostructure of dissimilar friction stir welding of aluminum alloys. Int J Dev Res 7(3):11884–11888. [http://www.journalijdr.com/mechanical-properties-and-macrostructure-dissimilar-friction-stir-welding-aluminum-alloys]

8. Elfar OMR, Rashad RM, Megahed H (2016) Process parameters optimization for friction stir welding of pure aluminium to brass (CuZn30) using Taguchi technique. MATEC Web of Conferences 43(2016):03005. https://doi.org/10.1051/matecconf/20164303005

9. Mehta KP, Badheka VJ (2016) A review on dissimilar friction stir welding of copper to aluminum: process, properties, and variants. Mater Manuf Processes 31:233–254. https://doi.org/10.1080/10426914.2015.1025971

10. Abd MM, Elnabi TA, Osman AE, Mokadem AB, Elshalakany, (2022) Evaluation of the formation of intermetallic compounds at the intermixing lines and in the nugget of dissimilar steel/aluminum friction stir welds. J Market Res 9(5):10209–10222. https://doi.org/10.1016/j.jmrt.2020.07.027

11. Abd Elnabi MM, Osman TA, El Mokadem AE (2018) Mechanical properties and microstructure of dissimilar friction stir welding of pure aluminum to low carbon steel. Adv J Grad Res 4(1):47–58. https://doi.org/10.21467/ajgr.4.1.47-58

12. Yang P, Mao Y, Xu Y et al (2022) Interface characteristics, microstructure, and mechanical properties of friction stir lap welded dissimilar Al/Mg alloy joints: effect of pin-tip profile. Int J Adv Manuf Technol. https://doi.org/10.1007/s00170-021-08611-0

13. Ma Z, Sun X, Ji S et al (2021) Influences of ultrasonic on friction stir welding of Al/Ti dissimilar alloys under different welding conditions. Int J Adv Manuf Technol 112:2573–2582. https://doi.org/10.1007/s00170-020-06481-6

14. Silva ACF, Braga DFO, de Figueiredo MAV et al (2015) Ultimate tensile strength optimization of different FSW aluminium alloy joints. Int J Adv Manuf Technol 79:805–814. https://doi.org/10.1007/s00170-015-6871-2

15. J. Edwin Raja Dhas, S. Jenkins Hexley Dhas, (2012) A review on optimization of welding process. Proc Eng 38:544–554. https://doi.org/10.1016/j.proeng.2012.06.068

16. Gunaraj V, Murugan N (1999) Application of response surface methodology for predicting weld bead quality in submerged arc welding of pipes. J Mater Process Technol 88(1–3):266–275. https://doi.org/10.1016/S0924-0136(98)00405-1

17. Woolf PJ (2009) Chemical process dynamics and controls: pp.724. University of Michigan Engineering Controls Group

18. Anil Kumar KS, Murigendrappa SM, Kumar H (2017) A bottom-up optimization approach for friction stir welding parameters of dissimilar AA2024-T351 and AA7075-T651 alloys. J of Materi Eng and Perform 26:3347–3367. https://doi.org/10.1007/s11665-017-2746-z

19. Babu N, Karunakaran N, Balasubramanian V (2017) A study to estimate the tensile strength of friction stir welded AA 5059 aluminium alloy joints. Int J Adv Manuf Technol 93:1–9. https://doi.org/10.1007/s00170-015-7391-9

20. Ramaraju RV, Ibrahim AB, Mansor MA, Yattapu Y (2014) Structural properties of similar and dissimilar aluminum alloy joints by FSW. Proceedings of the ASME 2014 International Mechanical Engineering Congress and Exposition. Volume 2B: Advanced Manufacturing. Montreal, Quebec, Canada. November 14–20. V02BT02A002. ASME. https://doi.org/10.1115/IMECE2014-36960

21. Murali Krishna P, Ramanaiah N, Prasada Rao K (2013) Optimization of process parameters for friction stir welding of dissimilar aluminum alloys (AA2024 -T6 and AA6351-T6) by using Taguchi method. Int J Ind Eng Comput 4(1):71–80. https://doi.org/10.5267/j.ijiec.2012.11.002

22. Lakshminarayaran AK, Balasubramanian V (2008) Process parameters optimization for friction stir welding of RDE-40 aluminium alloy using Taguchi technique. Trans Nonferrous Met Soc China 18(3):548–554. https://doi.org/10.1016/S1003-6326(08)60096-5

23. Chanakyan C, Sivasankar S, Meignanamoorthy M, Ravichandran M, Muralidharan T (2020) Experimental investigation on influence of process parameter on friction stir processing of AA6082 using response surface methodology. Mater Today: Proc 21(1):231–236. https://doi.org/10.1016/j.matpr.2019.05.384

24. Umanath K, Palanikumar K, Veeramalai Sankaradass K, Uma, (2021) Optimizations of friction stir welding process parameters of AA6063 Aluminium alloy by Taguchi technique. Mater Today: Proc 46(9):4008–4013. https://doi.org/10.1016/j.matpr.2021.02.539

25. Palanivel R, Koshy Mathews P, Murugan N (2013) Optimization of process parameters to maximize ultimate tensile strength of friction stir welded dissimilar aluminum alloys using response surface methodology. J Cent South Univ 20:2929–2938. https://doi.org/10.1007/s11771-013-1815-1

26. Venkateswarlu D (2015) P. Nageswara rao, M.M. Mahapatra, S.P. Harsha, and N.R. Mandal, Processing and optimization of dissimilar friction stir welding of AA 2219 and AA 7039 alloys. J of Materi Eng and Perform 24(12):4809–4824. https://doi.org/10.1007/s11665-015-1779-4

27. Jia H, Wu K, Sun Y et al (2021) Experimental research and process parameter optimization of high-speed friction stir welding. Int J Adv Manuf Technol 115:3829–3838. https://doi.org/10.1007/s00170-021-07369-9

28. Ahmadnia M, Shahraki S, Kamarposhti MA (2016) Experimental studies on optimized mechanical properties while dissimilar joining AA6061 and AA5010 in a friction stir welding process. Int J Adv Manuf Technol 87:2337–2352. https://doi.org/10.1007/s00170-016-8636-y

29. Simoncini M, Costa A, Fichera S, Forcellese A (2021) Experimental analysis and optimization to maximize ultimate tensile strength and ultimate elongation of friction stir welded AA6082 aluminum alloy. Metals 11(1):69. https://doi.org/10.3390/met11010069

30. Sefene EM, Tsegaw AA (2021) Temperature-based optimization of friction stir welding of AA 6061 using GRA synchronous with Taguchi method. Int J Adv Manuf Technol. https://doi.org/10.1007/s00170-021-08260-3

31. Sagheer-Abbasi Y, Ikramullah-Butt S, Hussain G et al (2019) Optimization of parameters for micro friction stir welding of aluminum 5052 using Taguchi technique. Int J Adv Manuf Technol 102:369–378. https://doi.org/10.1007/s00170-018-3138-8

32. Meengam C, Sillapasa K (2020) Evaluation of optimization parameters of semi-solid metal 6063 aluminum alloy from friction stir welding process using factorial design analysis. J Manuf Mater Proc 4(4):123. https://doi.org/10.3390/jmmp4040123

33. Balamurugan S, Jayakumar K, Subbaiah K (2021) Influence of friction stir welding parameters on dissimilar joints AA6061-T6 and AA5052-H32. Arab J Sci Eng 46:11985–11998. https://doi.org/10.1007/s13369-021-05773-7

34. Raj A, Pratap Kumar J, Melwin Rego A, Sunit Rout I (2021) Optimization of friction stir welding parameters during joining of AA3103 and AA7075 aluminium alloys using Taguchi method. Mater Today: Proc 46(7):7733–7739. https://doi.org/10.1016/j.matpr.2021.02.246

35. Hasan MM, Ishak M, Rejab M (2017) Influence of machine variables and tool profile on the tensile strength of dissimilar AA7075-AA6061 friction stir welds. Int J Adv Manuf Technol 90:2605–2615. https://doi.org/10.1007/s00170-016-9583-3

36. Vidal C, Infante V (2013) Optimization of FS welding parameters for improving mechanical behavior of AA2024-T351 joints based on Taguchi method. J of Materi Eng and Perform 22:2261–2270. https://doi.org/10.1007/s11665-013-0499-x

37. Haribalaji V, Sampath Boopathi M, Asif M (2022) Optimization of friction stir welding process to join dissimilar AA2014 and AA7075 aluminum alloys. Materials Today: Proceedings 50(5):2227–2234. https://doi.org/10.1016/j.matpr.2021.09.499

38. Abd Elnabi MM, Abdel-Mottaleb MM, Osman TA, El Mokadem A (2019) Influence of friction stir welding parameters on metallurgical and mechanical properties of dissimilar AA5454–AA7075 aluminum alloys. J Market Res 8(2):1684–1693. https://doi.org/10.1016/j.jmrt.2018.10.015

39. Vijaya Kumar P, Madhusudhan Reddy G, Srinivasa Rao K (2015) Microstructure, mechanical and corrosion behavior of high strength AA7075 aluminium alloy friction stir welds – Effect of post weld heat treatment. Def Technol 11(4):362–369. https://doi.org/10.1016/j.dt.2015.04.003

40. Davis JR (2001) Alloying: understanding the basics. ASM International p 351–416. https://doi.org/10.1361/autb2001p351

41. ASTM B557–15 (2015) Standard test methods for tension testing wrought and cast aluminum- and magnesium-alloy products ASTM International, West Conshohocken, PA. https://doi.org/10.1520/B0557-15

42. ASM handbook: Vol. 9 (2004) Metallography and microstructures. ASM International, Materials Park, OH. https://doi.org/10.31399/asm.hb.v09.9781627081771

43. Park SH, Kim JJ (1997) Quality engineering using robust design and analysis. In: Kitsos C.P., Edler L. (eds) Industrial statistics. Contributions to Statistics: pp 3–15. Physica Heidelberg. https://doi.org/10.1007/978-3-642-59268-3_1

44. Zarepour H, Tehrani AF, Karimi D et al (2007) Statistical analysis on electrode wear in EDM of tool steel DIN 1.2714 used in forging dies. J Mater Process Technol 187–188:711–714. https://doi.org/10.1016/j.jmatprotec.2006.11.202

45. Longhurst WR, Strauss AM, Cook GE, Cox CD, Hendricks CE, Gibson BT, Dawant YS (2010) Investigation of force-controlled friction stir welding for manufacturing and automation. Proc. IMechE Part B: J Eng Manuf 224(6):937–949. https://doi.org/10.1243/09544054JEM1709

46. MohammadiSefat M, Ghazanfari H, Blais C (2021) Friction stir welding of 5052–H18 aluminum alloy: modeling and process parameter optimization. J of Materi Eng and Perform 30:1838–1850. https://doi.org/10.1007/s11665-021-05499-5

47. Rajakumar S, Muralidharan C, Balasubramanian V (2011) Influence of friction stir welding process and tool parameters on strength properties of AA7075-T 6 aluminium alloy joints. Mater Des 32(2):535–549. https://doi.org/10.1016/j.matdes.2010.08.025

48. Zhang Z, Wu Q, Gruijicic M, Wan ZY (2015) Monte Carlo simulation of grain growth and welding zones in friction stir welding of AA6082-T6. J Mater Sci 51:1882–1895. https://doi.org/10.1007/s10853-015-9495-x

49. Kumar K, Kailas SV (2008) The role of friction stir welding tool on material flow and weld formation. Mater Sci Eng A 485(1):367–374. https://doi.org/10.1016/j.msea.2007.08.013

50. Meilinger Á, Török I (2013) The importance of friction stir welding tool. Prod Proc Syst 6(1):25–34. http://midra.uni-miskolc.hu/JaDoX_Portlets/documents/document_15325_section_7840.pdf

51. Msomi V, Mabuwa S (2020) Analysis of material positioning towards microstructure of the friction stir processed AA1050/AA6082 dissimilar joint. Advances in Industrial and Manufacturing Engineering 1:1–8. https://doi.org/10.1016/j.aime.2020.100002

52. Guo JF, Chen HC, Sun CN, Bi G, Sun Z, Wei J (2014) Friction stir welding of dissimilar materials between AA6061 and AA7075 Al alloys effects of process parameters. Mater Des 56:185–192. https://doi.org/10.1016/j.matdes.2013.10.082

53. Park SK, Hong ST, Park JH, Park KY, Kwon YJ, Son HJ (2010) Effect of material locations on properties of friction stir welding joints of dissimilar aluminium alloys. Sci Technol Weld Joining 15(4):331–336. https://doi.org/10.1179/136217110X12714217309696

54. Rodriguez RI, Jordon JB, Allison PG, Rushing T, Garcia L (2015) Microstructure and mechanical properties of dissimilar friction stir welding of 6061-to-7050 aluminum alloys. Mater Des 83:60–65. https://doi.org/10.1016/j.matdes.2015.05.074

55. Dinaharan I, Kalaiselvan K, Vijay SJ, Raja P (2012) Effect of material location and tool rotational speed on microstructure and tensile strength of dissimilar friction stir welded aluminum alloys. Arch Civil Mech Eng 12(4):446–454. https://doi.org/10.1016/j.acme.2012.08.002

56. Priya R, Subramanya Sarma V, Prasad RK (2009) Effect of post weld heat treatment on the microstructure and tensile properties of dissimilar friction stir welded AA 2219 and AA 6061 alloys. Trans Indian Inst Met 62:11–19. https://doi.org/10.1007/s12666-009-0002-4

57. Kalemba-Rec I, Kopyściański M, Miara D et al (2018) Effect of process parameters on mechanical properties of friction stir welded dissimilar 7075–T651 and 5083–H111 aluminum alloys. Int J Adv Manuf Technol 97:2767–2779. https://doi.org/10.1007/s00170-018-2147-y

58. Elangovan K, Balasubramanian V (2007) Influences of pin profile and rotational speed of the tool on the formation of friction stir processing zone in AA 2219 aluminium alloy. Mater Sci Eng A 459(1–2):7–18. https://doi.org/10.1016/j.msea.2006.12.124

59. Lang X, Wagner G, Eifler D (2011) Microstructure and mechanical properties of friction stir welded AA5454 – joints. Friction Stir Welding and Processing VI. https://doi.org/10.1002/9781118062302.ch16

60. Ditzel PJ (1997) Microstructure/property relationships in aluminum friction stir welds [Master's thesis, Ohio State University]. http://rave.ohiolink.edu/etdc/view?acc_num=osu1381145015

61. Padmanaban G, Balasubramanian V (2009) Selection of FSW tool pin profile, shoulder diameter and material for joining AZ31B magnesium alloy—an experimental approach. Mater Des 30(7):2647–2656. https://doi.org/10.1016/j.matdes.2008.10.021

62. Ramanjaneyulu K, Madhusudhan Reddy G, Venugopal Rao A (2014) A. Role of tool shoulder diameter in friction stir welding: an analysis of the temperature and plastic deformation of AA 2014 aluminium alloy. Trans Indian Inst Met 67:769–780. https://doi.org/10.1007/s12666-014-0401-z

63. Wei W, González S, Hashimoto T, Abuaisha RR, Thompson GE, Zhou X (2016) In-service sensitization of a microstructurally heterogeneous AA5083 alloy. Mater Corros 67(4):378–386. https://doi.org/10.1002/maco.201508507

64. Kalemba-Rec I, Wróbel M, Kopyscianski M (2016) Investigations of friction stir welds between 5083 and 7075 aluminum alloys using EBSD and X-ray techniques. Acta Phys Pol, A 130(4):996–999. https://doi.org/10.12693/APhysPolA.130.996

65. Bala Srinivasan P, Dietzel W, Zettler R, dos Santos JF, Sivan V (2005) Stress corrosion cracking susceptibility of friction stir welded AA7075–AA6056 dissimilar joint. Mater Sci Eng A 392(1–2):292–300. https://doi.org/10.1016/j.msea.2004.09.065

66. Cavaliere P, De Santis A, Panella F, Squillace A (2009) Effect of welding parameters onmechanical and microstructural properties of dissimilar AA6082–AA2024 joints produced by friction stir welding. Mater Des 30(3):609–616. https://doi.org/10.1016/j.matdes.2008.05.044

67. Shigematsu I, Kwon YJ, Suzuki K, Imai T, Satio N (2003) Joining of 5083 and 6061 aluminum alloys by friction stir welding. J Mater Sci Lett 22:353–356. https://doi.org/10.1023/A:1022688908885

68. Zadpoor AA, Sinke J, Benedictus R (2009) Fracture mechanism of aluminium friction stir welded blanks. Int J Mater Form 2:319–322. https://doi.org/10.1007/s12289-009-0512-y